

1
2
3
4 1 ***In vitro* experiments and infrared spectroscopy analysis of acid and alkaline**
5
6 2 **phosphatases inhibition by vanadium complexes**
7
8
9 3
10 4
11
12
13

14 5 Juliana E. Parente^a, Luciana G. Naso^a, Khalil Jori^a, Carlos A. Franca^a, Ana Maria da Costa
15 6 Ferreira^b, Patricia A.M. Williams^a, Evelina G. Ferrer^{a,*}
16
17
18
19 7
20
21

22 8 ^aCenter of Inorganic Chemistry (CEQUINOR, CONICET-CICPBA-UNLP)-Department of
23 9 Chemistry-Faculty of Exact Sciences, National University of La Plata, Boulevard 120 e/ 60
24 10 y 64 (B1900AVV), 1900 La Plata, Argentina.

25 11 ^bDepartment of Fundamental Chemistry, University of São Paulo, Av. Prof. Lineu Prestes,
26 12 748, 05508-000 São Paulo, SP, Brazil.
27
28
29
30
31
32
33
34
35
36
37
38
39
40
41
42
43
44
45
46
47
48
49
50
51
52
53
54
55

56 22 To whom correspondence should be addressed (e-mail: evelina@quimica.unlp.edu.ar,
57 23 Phone: 54 0221 4259485, Fax: 54 0221 445-4393). ORCID: 0000-0002-6343-5170.
58
59
60

24 **Abstract**View Article Online
DOI: 10.1039/C9NJ01638D

25
26 In the course of our research of vanadium-containing complexes, two oxidovanadium
27 complexes containing vanadium(V) and (IV) core with 4-aminobenzoic acid and/or peroxy
28 anion as ligands were synthesized and characterized by elemental analysis, conductivity
29 measurements, thermogravimetric analysis, and ¹H NMR, EPR, FTIR, UV/Vis
30 spectroscopies. Their compositions and geometrical structures
31 ($[[VO(O_2)(C_7H_6NO_2)(H_2O)] \cdot H_2O$, $[VO(C_7H_6NO_2)_2H_2O]$) were supported by experimental
32 data and theoretical studies (Density functional theory, DFT). The complexes were
33 evaluated *in vitro* as phosphatase inhibitors (alkaline and acid enzymes) being considered
34 as potential pharmaceutical agents under over-expression of those biochemical markers.
35 The effect achieved was then analysed through FTIR spectroscopy. Changes in the finger
36 print substrate bands as well as induced conformational changes on phosphatases enzymes
37 secondary structure were further examined. Eventually albumin interactions experiments
38 were performed in order to derive their bioavailability.

39
40 **Keywords:** vanadium complexes, phosphatase inhibition, FTIR spectroscopy, secondary
41 structure.

42

43

44

45

46

1. Introduction

Over recent years, several developments in the field of medicinal bioinorganic chemistry have taken place leading to transformations in parent drugs distribution through structural modifications of the pharmacological ligands by means of preparation of corresponding metal-based drugs. Transition metal complexes in particular present considerably more advantages compared to organic-based drugs due to the variability seen regarding coordination numbers, geometries, redox states, ligand substitution and structural diversity. Coordination to a metal ion usually leads to charge addition, and specific conformations that often ameliorate the biological activity of organic-based drugs. This novel strategy for therapy or diagnosis has come to the forefront.^{1,2} There are many examples in which a synergistic effect is observed resulting in improved biological activity. Vanadium is included in this large list of metals with physiological roles; and it can be in its higher oxidation states V (V, d^0) and V (IV, d^1) in biological systems forming anionic or cationic complexes at physiological pH. Those oxidation states easily convert to each other playing an important role in the balance of reactive oxygen species which determine their intra or extra-cellular composition. In solution, vanadium exhibits rich chemistry along with its redox behaviour including the ability to form complexes with a great variety of biological molecules (ATP, ribose, glutathione, amino acids, etc). Vanadium chemical affinity to oxygen, nitrogen or sulphur atoms, as well as its flexibility in coordination geometry (tetrahedral, octahedral, to trigonal pentagonal-bipyramid for V(V), and also square pyramidal for V(IV)) allows it to form stable or transition state complexes to participate in biological process.^{3,4} It was not until the 1960s that vanadium chemistry and biochemistry attracted interest with two major aspects being considered: first, biological systems and vanadium-based compounds have pharmaceutical and industrial applications; second,

1
2
3 72 vanadium coordination complexes have further been recognized as efficient catalysts in
4 several oxidation processes of industrial interest⁵ including vanadium(V) oxo and peroxy
5
6 73 complexes containing ligands similar to 4-aminobenzoic acid.⁶ Vanadium compounds have
7
8 74 been studied in relation to their pharmacological activities including antihyperlipidemic,
9
10 75 anti-obesity, diuretic, antihypertensive and anticancer drugs, among others.^{3,4} It was the
11
12 76 vanadium antidiabetic effect in particular which has been attributed to the structural
13
14 77 similarity between phosphate and vanadate anions. As a consequence, several vanadium
15
16 78 species and organic derived compounds were successfully proven as antidiabetic agents.
17
18 79 Their actions may include (i) enhancement of the glucose transport, (ii) inhibition of
19
20 80 gluconeogenesis, lipolysis, and glycogenolysis in the liver and (iii) inhibition of protein
21
22 81 tyrosine phosphatase (PTPase) and alkaline phosphatase (ALP). In this sense, vanadium
23
24 82 dipicolinate complexes were proven to behave as insulin-mimetic compounds.^{7,8}
25
26 83
27
28 84 Phosphatases display a number of physiological functions and their selective inhibitors
29
30 85 have potential therapeutic roles. PTP1B (Protein tyrosine phosphatases 1B) belongs to a
31
32 86 family of enzymes that catalyse the dephosphorylation of tyrosine (Tyr)-phosphorylated
33
34 87 proteins. This phosphatase is involved in the deregulation of insulin and leptin signals
35
36 88 which show significant for diabetes and obesity. These are part of the reasons why PTP1B
37
38 89 becomes a therapeutic target encouraging selective inhibitors research.⁹ There are many
39
40 90 examples including alkaline (ALP) and acid (AcP) phosphatases. While the over-
41
42 91 expression of non-specific alkaline phosphatase tissue is associated with hypophosphatasia,
43
44 92 hydroxyapatite deposition disorder, vascular and arterial calcification, and hyperthyroidism
45
46 93 condition¹⁰, the elevated levels in serum of acid phosphatase are on the contrary correlated
47
48 94 with osteoporosis and metabolic bone malignancies as well as cancer with bone metastases.
49
50 95 AcP has indeed been identified as a relevant drug target for the treatment of bone-
51
52 96 associated diseases.¹¹
53
54
55
56
57
58
59
60

1
2
3 97 Vanadium species are recognized as phosphatase inhibitors. Orthovanadate (VO_4^{3-})
4 behaves as a strong inhibitor of Na^+ , K^+ -ATPase, PTPase and ALP and also of potato and
5
6 98
7
8 99 wheat germ acid phosphatases.¹² Despite the great effect showed by vanadium species,
9
10 100 reported side effects prompted researchers to prove others vanadium organic derivative
11
12 101 compounds as inhibitors. In effect it can be seen in the literature ^{3,12} that several vanadium
13
14 102 compounds have been tested as phosphatase inhibitors. They mainly included
15
16 103 oxidovanadium(V) and (IV) cations and bisperoxidovanadium complexes; reports
17
18 104 pertaining to peroxidovanadium complexes, specifically those concerning AcP are,
19
20 105 however, scarce.

21
22
23
24 106 All these observations encourage us to prepare, characterize and test *in vitro* the behaviour
25
26 107 of two vanadium complexes with 4-aminobenzoic acid as ligand, based in the sequential
27
28 108 interest of our research group in the development and study of new phosphatase inhibitors
29
30 109 with promising bioactivities.

31
32
33
34 110 Finally, studies on protein carrier using fluorescence albumin experiments were performed
35
36 111 in order to assess if the complexes can interact and be delivered by albumin at
37
38 112 physiological conditions.

39
40
41 113

42 43 114 **2. Materials and methods**

44
45
46 115

47
48
49 116 Vanadium(V) oxide (Anedra), solid oxidovanadium(IV) sulfate pentahydrate (Merck) and
50
51 117 4-aminobenzoic acid (Acros Organics) were used as supplied. Peroxido species was
52
53 118 prepared according to Fantus *et al.*¹³ Bovine Serum Albumin BSA (A-6003, essentially
54
55 119 fatty acid-free), bovine intestinal ALP (EC 3.13.1, calf intestinal mucose) and acid
56
57 120 phosphatase AcP (EC 3.1.3.2, potato source) were obtained from Sigma Chemical
58
59
60

1
2
3 121 Company (St. Louis, MO) and used as supplied. All the chemicals used were from
4 analytical grade. Elemental analysis for carbon, nitrogen and hydrogen was performed
5
6 122 analytical grade. Elemental analysis for carbon, nitrogen and hydrogen was performed
7
8 123 using a Carlo Erba EA1108 analyzer. Vanadium content was determined by the
9
10 124 tungstophosphovanadic method. A Shimadzu system (model TG-50 and DTA-50),
11
12 125 working in an oxygen flow of 50 mL.min⁻¹ and at a heating rate of 10 °C.min⁻¹ has been
13
14 126 used for the thermogravimetric analysis. Sample quantities ranged between 10 and 20 mg.
15
16 127 Al₂O₃ was used as a DTA standard.

17
18
19 128 FTIR spectra of powdered samples as pressed KBr pellets were measured with a
20
21 129 Bruker IFS 66 FTIR-spectrophotometer in the 4000-400 cm⁻¹ wavenumber range. Spectra
22
23 130 were recorded with a wavenumber resolution of 4 cm⁻¹ and 64 scans were averaged for
24
25 131 each spectrum. The data were analyzed using OPUS program (Bruker Optics, USA).

26
27
28 132 EPR spectra in solid state were registered in an EMX Bruker instrument, working at
29
30 133 X-band, at low temperature (77K) or at room temperature (298K). DPPH was used as
31
32 134 calibrant. Usual instrument parameters: Power = 20.17 mW; frequency 9.42 GHz;
33
34 135 modulation frequency 100 MHz; modulation amplitude 15G; time constant 20.48 ms.

35
36
37 136 UV/Vis spectra were recorded with a Shimadzu 2600/2700 spectrophotometer. This
38
39 137 instrument was also used to collect the diffuse reflectance spectra, employing MgO as a
40
41 138 standard for those experiments. Fluorescence spectra were obtained using a Shimadzu
42
43 139 (RF6000) luminescence spectrometer equipped with a pulsed xenon lamp.

44
45
46 140

47 141 **2.1. Syntheses of complexes**

48
49 142

50
51 143 **[VO(O₂)L(H₂O)].H₂O (L= C₇H₆NO₂)**

52
53 144

1
2
3 145 Vanadium(V) oxide (0.099 g; 0.54 mmol) was dissolved in 10 ml of hot water by adding
4
5 146 KOH 1M with heating and stirring until complete dissolution. The resulting clear yellow
6
7 147 solution was stirred at 0°C and the pH was adjusted at 4 (with drops of HCl 1M). To this
8
9 148 solution, 0.15 g (1.1 mmol) of 4-aminobenzoic acid dissolved in 25 ml of distilled water
10
11 149 was added followed by the addition of 3 mL of 10% H₂O₂ to give a red solution. The
12
13 150 solution was left stirring (24h) and its volume was reduced by evaporation of the solvent at
14
15 151 60°C to ca. 70%. The precipitated brownish orange powder was filtered out and allowed to
16
17 152 dry at room temperature. Elemental analysis: Calc.: 31.46% C, 5.24% N, 3.74% H, 19.10%
18
19 153 V; Exp.: 31.08% C, 4.98% N, 3.66% H, 18.81% V. TG curve: loss of one water molecule
20
21 154 up to 160 °C ($\Delta\omega_{\text{exp}} = 5.98\%$ and $\Delta\omega_{\text{calc}} = 6.74\%$, DTA, endo 50 °C). This temperature is
22
23 155 indicative that the water molecule is not bonded to the metal, being hydration water. The
24
25 156 complex is soluble in DMSO and DMF, partially in other organic solvents and insoluble in
26
27 157 H₂O. For the biological measurements the complex was initially dissolved in DMSO and,
28
29 158 thereafter a solution of the complex in a mixture of DMSO:water (5% in DMSO) was used.
30
31 159 The values of the molar conductivities were: $\Omega = 16.2 \text{ S.cm}^2.\text{mol}^{-1}$ ($7.14 \times 10^{-4} \text{ M}$,
32
33 160 methanol) and $\Omega = 21.69 \text{ S.cm}^2.\text{mol}^{-1}$ ($5.53 \times 10^{-4} \text{ M}$, DMF). It can be considered that the
34
35 161 compound do not dissociate in solution, since for a 1:1 electrolyte, the Ω values should be
36
37 162 $\geq 70 \text{ S.cm}^2.\text{mol}^{-1}$ in those solvents.¹⁴ ¹H NMR spectra: Exp (Calc): H aromatic: H2a=7.72
38
39 163 (7.73) ppm, H3a=6.62(6.25) ppm, H5a= 6.65(6.31) ppm, H6a=7.75(7.55) ppm.¹⁵
40
41
42
43
44
45
46
47
48
49
50

51 165 **[VOL₂H₂O] (L= C₇H₆NO₂)**
52
53
54 166

55
56 167 To obtain this complex, 0.253 g (1 mmol) of VOSO₄·5H₂O were dissolved in 5mL of
57
58 168 distilled water. It was then dropwise added to a solution of 0.274 g (2 mmol) of 4-

1
2
3 169 aminobenzoic acid dissolved in 45 mL of distilled water. To this solution, an aqueous
4
5 170 NaOH 1M solution was added, under continuous stirring to a final pH value of 5. The
6
7 171 resulting dark green solution was kept under stirring for 4 h. After that, a green precipitate
8
9 172 was formed which was separated by centrifugation, washed several times and dried in an
10
11 173 oven (60 °C). Elemental analysis: Calc.: 47.06 %C, 7.84 %N, 3.92 %H, 14.28 %V; Exp:
12
13 174 47.52 %C, 8.20 %N, 3.70 %H, 14.25 %V. TG curve: one water molecule is lost at 180 °C
14
15 175 ($\Delta\omega_{\text{exp}} = 4.87\%$ and $\Delta\omega_{\text{calc}} = 5.04\%$, DTA, endo). In this case the high dehydration
16
17 176 temperature value indicated that the water molecule is coordinated to the metal ion. The
18
19 177 values of the molar conductivities were: $\Omega=18.9\text{ S}\cdot\text{cm}^2\cdot\text{mol}^{-1}$ ($7.14 \times 10^{-4}\text{ M}$, methanol) and
20
21 178 $\Omega=33.55\text{ S}\cdot\text{cm}^2\cdot\text{mol}^{-1}$ ($4.47 \times 10^{-4}\text{ M}$, DMF). It can be considered that the compound do not
22
23 179 dissociate in solution, since for a 1:1 electrolyte, the Ω values should be $\geq 70\text{ S}\cdot\text{cm}^2\cdot\text{mol}^{-1}$ in
24
25 180 those solvents.¹⁴ ¹H NMR spectra: Exp (Calc): H aromatic: H2a=7.72 (7.44) ppm,
26
27 181 H2a'=7.72 (7.58) ppm, H3a=6.62(6.23) ppm, H3a'=6.62(6.19) ppm, H5a= 6.65(6.25) ppm,
28
29 182 H5a'= 6.65(6.30) ppm, H6a=7.75(7.60) ppm , H6a'=7.75(7.67) ppm.¹⁵
30
31
32
33
34
35
36
37
38
39
40
41
42
43
44
45
46
47
48
49
50
51
52
53
54
55
56
57
58
59
60

184 2.2. Phosphatases Inhibition. *In vitro* assays.

185 Acid phosphatase

186
187 Acid phosphatase inhibition test was performed according to Blum and Schwedt
188 procedures.¹⁶ The compounds solutions were prepared by diluting the stock solutions
189 prepared in DMSO with acetate buffer (pH=5.6) to give final concentrations of 10 to 500
190 μM . A volume of 0.50 mL of complex solution (10-500 μM) was mixed with 0.10 mL of
191 the enzyme solution and 1.00 mL of buffer. The mixture was kept at 37°C for 20 min
192 (incubation time). After starting the reaction by adding 0.10 mL of the substrate solution

1
2
3 193 (*p*-nitrophenylphosphate (*p*-NPP)), the tube was kept at 37°C for more 20 min. The
4
5 194 reaction was stopped with the addition of 0.50 mL of a 0.5 M sodium hydroxide solution.
6
7 195 The enzymatic activity was finally calculated by measuring the absorbance of *p*-
8
9 196 nitrophenol at 405 nm against a blank prepared without the enzyme. Three independent
10
11 197 replicates of each point were measured. The 100% of the enzyme activity is assigned to a
12
13 198 basal measurement containing all the reaction media including the same volume of DMSO
14
15 199 in all the experiments. It is worthy to mention that the presence of DMSO (0.5%) did not
16
17 200 affect the enzyme activity.
18
19
20
21
22
23
24

201

202 **Alkaline phosphatase**

203

204 The basis of the method is similar to that of AcP but differs in the pH value of the reaction
205 medium. Again, the conversion of the substrate *p*-NPP to *p*-nitrophenol was monitored by
206 the absorbance changes at 405 nm. Briefly, the experimental conditions for ALP specific
207 activity measurement were as follows: 1 µg/mL of bovine intestinal ALP and 5 mM of *p*-
208 NPP were dissolved in the incubation buffer (55 mM glycine +0.55 mM MgCl₂, pH=10.5)
209 and held for 10 min. The effects of the compounds were determined by addition of
210 different concentrations (10-500 µM) of each one to the pre-incubated mixture. The
211 solutions of the complexes were prepared in DMSO before adding the buffer to obtain the
212 desired final concentrations. The effect of each concentration was tested at least in
213 triplicate in three different experiments.

214

1
2
3 215 **2.3 Infrared spectroscopy: analysis of the substrate (*p*-nitrophenylphosphate)**
4
5 216 **vibrational bands and the secondary structure of the phosphatases at the inhibition**
6
7 217 **experimental conditions.**
8
9

10 218
11
12
13 219 For the substrate analysis, FTIR spectra of the freeze-dried powdered samples were
14
15 220 collected. The samples were prepared at the same experimental conditions than the *in vitro*
16
17 221 experiments. Then, to investigate the ability of the compounds to produce conformational
18
19 222 changes in the phosphatases enzymes, solution spectra were measured under the same
20
21 223 experimental conditions of inhibitory experiments but without the addition of p-NPP. FT-
22
23 224 IR/ATR spectra were recorded with a Bruker IFS 66 FTIR-spectrophotometer from 4000
24
25 225 to 400 cm⁻¹ equipped with an internal reflectance accessory using ZnSe crystal designed to
26
27 226 have one angle of light incidence of 45°. Spectra were recorded at room temperature with a
28
29 227 spectral resolution of 4 cm⁻¹. To improve the signal-to-noise ratio, 200 scans were averaged
30
31 228 for each spectrum and the procedure was performed as reported previously.¹⁷ According to
32
33 229 the results obtained in the previous section, the FTIR/ATR spectra of the buffer solutions
34
35 230 (acetate buffer and glycine for AcP and ALP, respectively), AcP and ALP (at the same
36
37 231 concentrations as the inhibition tests) and the systems: (i) ALP with 4-aminobenzoic acid
38
39 232 (500 μM), V(IV)O²⁺ (250 μM), oxidovanadium(IV) (500 μM) and peroxidovanadium(V)
40
41 233 compounds (500 μM), (ii) AcP with 4-aminobenzoic acid (500 μM), V(IV)O²⁺ (250 μM),
42
43 234 oxidovanadium(IV) (250 μM) and peroxidovanadium(V) (500 μM) compounds were taken
44
45 235 independently, and analyzed. Then, the absorbance values of the buffer solution were
46
47 236 subtracted from the values of the protein solution to get the FT-IR spectra of the protein.
48
49 237 All spectra were vector normalized in the whole range (4000-500 cm⁻¹) and were obtained
50
51 238 after collecting and averaging 200 scans. All analyses were performed in three independent
52
53 239 experiments, and the results were reported as averages of these replicates. The
54
55
56
57
58
59
60

1
2
3 240 determination of the secondary structure was carried out on the basis of the procedure
4
5 241 previously described.¹⁷ The Amide I region (1700-1600 cm⁻¹) was used to investigate the
6
7 242 secondary structure of the phosphatases in a quantitative manner. The frequencies, the
8
9 243 number of peaks to be fitted, and the half-width of each peak to start a least square iterative
10
11 244 curve-fitting procedures were those obtained from the second derivative of the original
12
13 245 spectra. The areas of the bands were calculated by integration of the corresponding fitted
14
15 246 band. A straight baseline passing through the ordinates at 1700 cm⁻¹ and 1600 cm⁻¹ was
16
17 247 adjusted as an additional parameter to obtain the best fit. The curve-fitting procedure was
18
19 248 performed by stepwise iterative adjustment towards a minimum root mean-square error of
20
21 249 the different parameters determining the shape and position of the absorption peaks. It was
22
23 250 carried out by assuming an initial mixed Lorentzian-Gaussian line-shape function, with full
24
25 251 width band at half height (FWHH) of 10-15 cm⁻¹ and a maximum resolution factor.
26
27 252 Baseline corrections, normalization, derivation, curve fitting and area calculation were
28
29 253 carried out by means of Grams/32 (Galactic Industries Corporation, USA) software, OPUS
30
31 254 3.1, and Perkin-Elmer software. The resulting fitted curve was analyzed taking into
32
33 255 account the following assignments: β -sheets, 1637-1613 cm⁻¹; solvated helix, 1625-1637
34
35 256 cm⁻¹, random coil, 1645-1637 cm⁻¹, α -helix, 1658-1650 cm⁻¹, turns, 1673-1666 cm⁻¹ and β -
36
37 257 antiparallel, 1695-1675 cm⁻¹. In order to calculate the percentage contribution of the
38
39 258 different types of conformations to the area of all the components, bands assigned to a
40
41 259 given conformation were summed and divided by the total Amide I area.
42
43
44
45
46
47
48
49
50
51

260

261 **2.4. Albumin interaction**

262

263 **Fluorescence quenching experiments**

264

1
2
3 265 Bovine serum albumin (BSA) was dissolved in 0.1M Tris-HCl buffer (pH 7.4) to attain a
4
5 266 final concentration of 6 μM . The solutions of the studied compounds were added drop-wise
6
7 267 to the above 6 μM BSA preparation to ensure the formation of a homogeneous solution and
8
9 268 to obtain the desired concentration of 0-100 μM . Adequate solubility was reached under
10
11 269 these experimental conditions and the compounds did not showed significant fluorescence
12
13 270 that could interfere with the measurements. For each sample and concentration, three
14
15 271 independent replicates were performed at 25 $^{\circ}\text{C}$ and 37 $^{\circ}\text{C}$. BSA 6 μM was titrated by
16
17 272 successive additions of complex solutions from 0 to 100 μM and the fluorescence intensity
18
19 273 was measured (excitation at 280 nm and emission at 348 nm). All the fluorescence
20
21 274 quenching data were analyzed according to previous studies performed in the laboratory by
22
23 275 applying a traditional mathematical procedure. The fluorescence-quenching mechanism
24
25 276 has been analyzed using the Stern-Volmer eq. (1).¹⁸

$$277 \quad F^0/F = 1 + K_{sv} [Q] \quad \text{eq. (1)}$$

278 where F^0 is the steady-state fluorescence intensity of BSA alone while F is the observed
279 intensity upon increasing the quencher concentration, K_{sv} is the Stern-Volmer quenching
280 constant and $[Q]$ is the quencher concentration. Usually, the curve of F^0/F vs $[Q]$ is linear if
281 the type of quenching involves a unique process: static or dynamic. Static quenching is due
282 to the complex formation between the fluorophore and the quencher. It can be
283 distinguished from collision effects because generally the K_{sv} value is higher than the value
284 of the dynamic quenching constant (K_q). Considering that $K_q = K_{sv}/\tau_0$ (where $\tau_0 = 10^{-8}$ s is
285 the average lifetime of the biomolecule without quencher), this constant can be estimated
286 and compared with the maximum diffusion collision quenching rate constant (reference
287 value from the literature) which is $2 \times 10^{10} \text{ M}^{-1} \text{ s}^{-1}$. If the K_{sv} value is greater, then a
288 mechanism of interaction through the complex formation can be proposed. Otherwise it
289 would be a collisional quenching. If the quenching is static, it is assumed that there are

290 specific binding sites. These binding sites, and their association constants, were estimated
291 using the following mathematical relationship:

$$\log [(F^0-F)/F] = \log K_b + n \log [Q] \quad \text{eq. (2)}$$

293 where K_b is the binding constant and n is the average number of binding site per protein
294 molecule.

295 To obtain information about the type of interaction, the thermodynamic parameters were
296 calculated using Van't Hoff equation¹⁸:

$$\ln (K_{b2}/K_{b1}) = -\Delta H^0/R (1/T_2-1/T_1) \quad \text{eq. (3)}$$

298 where T_1 and T_2 are the absolute temperatures at which K_{b1} and K_{b2} were determined. The
299 standard free energy change (ΔG^0) and the standard free entropy change (ΔS^0) were
300 evaluated according to the well-known thermodynamic relationships:

$$\Delta G^0 = -RT \ln K_b \quad \text{eq. (4)}$$

$$\Delta S^0 = (\Delta H^0 - \Delta G^0)/T \quad \text{eq. (5)}$$

305 3D fluorescence spectra

306
307 The three-dimensional fluorescence spectra were performed under the following
308 experimental conditions: (i) Emission wavelength was recorded between 200 and 600 nm,
309 (ii) Excitation wavelength from 200-400 (5 nm of increment), (iii) the number of scanning
310 curves was 15. Other scanning parameters were just the same to those of the fluorescence
311 quenching spectra.

2.5. Computational methods

View Article Online
DOI: 10.1039/C9NJ01638D

313

314 The absence of X-ray single-crystal analysis led us to characterize the structures of
315 the complexes using Gaussian 09 program¹⁹ and the density functional theory (DFT)
316 calculations which have demonstrated a good correlation with experimental data for
317 coordination metal complexes. Truhlar model M06L²⁰ was used to optimize the geometries
318 based on a meta-GGA functional. Basis sets of triple-zeta quality with polarized (TZVP)
319 functions were used for all atoms. The initial structures of the complexes were modeled as
320 isolated molecules according to the experimental data for the complexes and taking into
321 account the solvent environment using the conducting polarizable continuous model
322 (CPCM) as implemented in the software package. The ground state geometries were
323 optimized using the method mentioned above in the gas phase. The vibrational analysis
324 were performed at the same level of theory in order to get a minimum on the potential
325 energy surface, and then, calculation of IR and Raman frequencies were considered for
326 supporting the characterization of the complexes. UV-vis spectra were calculated with the
327 time-dependent density functional theory (TD-DFT) formalism²¹ using the well-known
328 functional B3LYP^{22,23} and a split-valence triple zeta basis set (6-311+g*). Solution spectra
329 were carried out simulating solvent effect using the same model described above. Water
330 and DMF were taken into account for optimization and UV/Vis, respectively.

331

3. Results and discussion

333

334 Experimental data (elemental analysis, thermogravimetric, conductimetry, ¹H NMR),
335 physicochemical characterizations (see above) together with theoretical optimized
336 structures analysis, let us to propose the following structures to the studied complexes,

1
2
3 337 showed in Figure 1. In the peroxido complex $[\text{VO}(\text{O}_2)\text{L}(\text{H}_2\text{O})]\cdot\text{H}_2\text{O}$, the vanadium center
4
5 338 is located in a pentagonal pyramid with a bidentate coordination mode of the peroxo and
6
7 339 the carboxylate group of the 4-aminobenzoate ligand. A water molecule occupied the
8
9 340 equatorial position forming a distorted pentagonal plane (Figure 1A). For the
10
11 341 oxidovanadium complex *cis*- $[\text{VOL}_2\text{H}_2\text{O}]$, the oxidovanadium(IV) cation shows a distorted
12
13 342 octahedral structure being both 4-aminobenzoate ligands in a bidentate coordination mode
14
15 343 through the carboxylate groups and a water molecule complete the six-coordination sphere.
16
17 344 From the two calculated possible conformations (*cis*- and *trans*-) the *cis*-one was in
18
19 345 correspondence with the experimental results (see below), showed in Figure 1B (see Figure
20
21 346 S1 for *trans* structure). Characteristic bond lengths and angles around the vanadium atom
22
23 347 for the complexes are depicted in Table 1.
24
25 348

26 349 **3.1. Infrared Spectra**

27 350
28 351 The FTIR spectrum was analyzed in comparison with the corresponding spectrum of 4-
29
30 352 aminobenzoic acid which has been extensively studied.¹⁵ The most characteristic bands are
31
32 353 shown in Table 2. (Figure S2).

33 354 The FTIR spectra of the complexes display typical features of the coordinated
34
35 355 ligand when they were compared with the spectra of 4-aminobenzoic acid and its sodium
36
37 356 salt. The calculated spectra for $[\text{VO}(\text{O}_2)\text{L}(\text{H}_2\text{O})]\cdot\text{H}_2\text{O}$ and $[\text{VOL}_2\text{H}_2\text{O}]$ were used to
38
39 357 support empirical assignment of the vibrational bands. Table 2 shows that the experimental
40
41 358 and the selected calculated wavenumbers for the compounds are in good agreement even
42
43 359 without the use of scaling factors. The differences observed are related to the fact that the
44
45
46
47
48
49
50
51
52
53
54
55
56
57
58
59
60

1
2
3 360 calculations for the isolated molecule have been performed in gas phase and the
4
5 361 experimental spectra correspond to solid samples.
6
7

8 362 As it is well known, the formation of an ionic salt from a carboxylic acid produces
9
10 363 two bands related to the ionic form of the carboxylate group corresponding to the
11
12 364 asymmetric $\nu_{as}(\text{COO}^-)$ and symmetric $\nu_s(\text{COO}^-)$ stretching modes.²⁴ Thus, the 1680 cm^{-1}
13
14 365 band of the $\nu(\text{C}=\text{O})$ stretching of the carboxylic acid group is splitted into two components
15
16 366 at 1529 cm^{-1} and 1397 cm^{-1} in the sodium salt giving a $\Delta\nu$ ($\nu_{as}(\text{COO}^-)$ - $\nu_s(\text{COO}^-)$) value of
17
18 367 132 cm^{-1} . Other characteristic bands are due to the presence of the $-\text{NH}_2$ group in the
19
20 368 molecules of both (the free acid and the sodium salt). They appear in the ranges of 1620-
21
22 369 1635 cm^{-1} for the $\delta(\text{NH}_2)$ and 1070-1085 cm^{-1} for the $\delta(\text{HNC})$ vibrational modes.
23
24 370 Analyzing the FTIR spectrum of the *cis*-oxidovanadium(IV) complex, two new bands at
25
26 371 1506 cm^{-1} and 1408 cm^{-1} can be clearly seen. These bands can be assigned to the
27
28 372 asymmetric stretching ($\nu_{as}(\text{COO}^-)$) and symmetrical stretching ($\nu_s(\text{COO}^-)$) vibrational
29
30 373 modes, respectively. The same vibrational modes appear at 1525 cm^{-1} and 1429 cm^{-1} in the
31
32 374 peroxidovanadium(V) complex. In both cases the calculated $\Delta\nu$ values (98 and 96 cm^{-1} ,
33
34 375 respectively) are lower than the $\Delta\nu$ of the sodium salt suggesting a bidentate type of
35
36 376 coordination of the carboxylate group to vanadium.²⁴ In addition, the $\nu(\text{V}=\text{O})$ stretching
37
38 377 bands can be detected. They appear at 965 cm^{-1} for the oxidovanadium(IV) complex. It
39
40 378 was established that the decrease of $\nu(\text{V}=\text{O})$ stretching frequency which occurs in
41
42 379 oxidovanadium complexes is a measure of the donor ligand capacity. From the differences
43
44 380 observed between the calculated and experimental $\nu(\text{V}=\text{O})$ frequencies values of the
45
46 381 oxidovanadium(IV) complex, the lowest value is shown by the *cis*- configuration which
47
48 382 has a longer $\text{V}=\text{O}$ distance (see electronic supplementary information). This is in
49
50 383 correspondence with the presence of one water molecule in the equatorial plane of the
51
52 384 oxidovanadium(IV) complex having less electron donation ability than the carboxylate
53
54
55
56
57
58
59
60

385 group as it was expected.²⁵ For the peroxidovanadium(V) complex (with a shorter bond
386 length, see Table 1) this band can be detected at higher wavenumbers (998 cm⁻¹) and has
387 been assigned to a combined vibration of V=O and O-O bonds due to their mutual
388 interactions. Additionally, the vibrational modes corresponding to the characteristic
389 stretches $\nu(\text{V-O}_2)$ of the peroxy moiety can be assigned to the 668 and 630 cm⁻¹ bands
390 (associated to the deformation mode $\delta(\text{OOV})$ in the case of the lowest wavenumber).
391 These assignments agree well with previous studies for peroxido heteroligand vanadate
392 complexes.²⁶

393 The IR spectra of the complexes exhibit a broad absorption band in the 3300-3400 cm⁻¹
394 region and the νNH_2 vibration bands cannot easily be assigned. Thus, lower frequencies
395 of the FTIR spectra were analyzed. In relation to the presence of the NH₂ group in the
396 molecule, it is well known that the N-H bond in both, primary and secondary amines, are
397 polar having a partial charge density on H and a negative partial charge density on N. This
398 gives to the group the ability to form hydrogen bonds.²⁷ In the Table 2 (Figure S2), the
399 shifts of the bands assigned to vibrational modes of the NH₂ group can be observed.
400 According to the theoretical assignments, this band is actually composed of two
401 contributions $\delta(\text{NH}_2)$ and $\nu(\text{CC})$ (Table 2) with varying intensity ratios. For
402 $[\text{VO}(\text{O}_2)\text{L}(\text{H}_2\text{O})]\cdot\text{H}_2\text{O}$ the ratio is 3:1 $\delta(\text{NH}_2):\nu(\text{CC})$ in contraposition of the 1:1
403 relationship for $[\text{VOL}_2\text{H}_2\text{O}]$ and probably that is the reason why they appear with different
404 intensities in the FTIR spectra. In addition, the possibility of neighboring interactions
405 produced by the solid phase cannot be excluded. It can be noted that this combined band
406 shifted to higher wavenumber in comparison with the sodium salt and the ligand,
407 suggesting that the formation of the metallic complex provoked the rupture of the hydrogen
408 bonds causing the increment of the wavenumber values as a consequence of the shortening
409 of the NH bonds.²⁸

3.2. Diffuse reflectance and UV/Vis spectroscopy. Solution stability.

View Article Online
DOI: 10.1039/C9NJ01638D

The electronic spectra of the solids compounds and the behavior of the complexes in solution were studied using diffuse reflectance and UV-vis spectroscopy in order to characterize the complexes and to compare the species formed in solid phase with the species present in solution.

Both complexes behaved as expected in solid phase and in solution. The solid peroxidovanadium(V) complex showed the typical bands associated with the CT of the amino and peroxy groups which appear at c.a. 455 nm, 385 nm and 318 nm (460 nm, 392 nm and 314 nm from the fitting and deconvolution process; Figure 2(A) ((a) and (b), respectively).²⁹ It is well known that UV-vis spectroscopy is a very useful tool for identification of mono- or di- peroxido complexes. The absence of the peroxido-vanadium charge transfer band (c.a. 220 nm) implies the presence of the peroxido vanadium species. Usually, peroxidovanadium(V) complexes showed one absorption band in the region 400-460 nm and other CT band assigned to a L→M (peroxy to vanadium) (c.a. 325 nm) (Figure 2A(a)). In addition, the calculations performed (considering the solution spectra) support these assignments. Based on the theoretical calculations (Figure 2 (B, b)), the observed characteristic bands in the UV-vis spectra can be assigned as follow: 400 nm (HOMO → LUMO, H-1 → LUMO), ligand charge transfer (aminobenzene and peroxy) to metal; 342 nm (H-1→ L+2), ligand charge transfer (peroxy) to metal; 293 nm (H-1→ L+2, L+5), ligand charge transfer (peroxy) to ligand (aminobenzene) (Figure S3). The two last transitions are typical for peroxidovanadium species. Solution spectrum (2.7x10⁻³ M, DMF, Figure 2B(a)) showed similar pattern band with splitting of the band around 300 nm. The most intense bands are displayed at 303 nm ($\epsilon = 525.9 \text{ M}^{-1} \cdot \text{cm}^{-1}$), 330 nm ($\epsilon = 540.7 \text{ M}^{-1} \cdot \text{cm}^{-1}$) and 407 nm ($\epsilon = 129.6 \text{ M}^{-1} \cdot \text{cm}^{-1}$). Similar pattern was obtained from the fitting and

deconvolution process which is also consistent with the simulated solution spectrum (Figure 2 (A, B)).

The solid oxidovanadium(IV) complex usually shows d-d absorption bands. Three absorptions are expected: $b_2(dx y) \rightarrow e(dx z, dy z)$ (1000-670 nm), $b_2(dx y) \rightarrow b_1(dx^2 - y^2)$ (667-555 nm), $b_2(dx y) \rightarrow a_1(dz^2)$ (417-345 nm), being the last one usually overlapped for a charge transfer band from the ligand. In this case, the reflectance spectrum of the oxidovanadium(IV) complex showed two characteristic d-d bands, one located > 850 nm and other at 623 nm corresponding to the two lower energy transitions according to Ballhausen-Gray energy level scheme (Figure 3A).³⁰ Solution spectrum (0.11 M, DMF) showed bands at 400-900 nm region which can be assigned to the electronic d-d transitions of $b_2 \rightarrow b_1$ (480 nm, $\epsilon = 25.18 \text{ M}^{-1} \cdot \text{cm}^{-1}$) and $b_2 \rightarrow e$ (864 nm, $\epsilon = 27.54 \text{ M}^{-1} \cdot \text{cm}^{-1}$; 740 nm (shoulder, $\epsilon = 23.72 \text{ M}^{-1} \cdot \text{cm}^{-1}$) (Figure 3B). Solvent effect, possibly caused by the replacement of the water molecule in the equatorial position, or axial coordination around the metal center, provoked a blue shift of these bands in comparison with the solid reflectance spectrum. The *cis*- conformation for the oxidovanadium(IV) complex is additionally supported by the calculated *cis*-UV/Vis spectrum. The spectrum of the *cis*- conformation exhibits a good correlation with the experimental one (Figure 3C) having a similar pattern with two bands in opposition with the simulated for the *trans*-one. The observed splitting of the UV/Vis band is usually expected as a consequence of the symmetry lowering.³¹ According to the calculations, the bands were assigned to 733 nm (H-2 \rightarrow L) and 548 nm (H-2 \rightarrow L+4) and correlates reasonably well with the experimental spectrum (Figure S4).

Both complexes remained stable in a DMF and DMSO solutions (no appreciable changes were observed in the UV/Vis spectra, data not shown) at least during 1h. Then, it

459 can be stated that the complex did not decompose during the manipulation of the solutions
460 for the *in vitro* biological assays.

461

462 3.3. EPR spectroscopy

463

464 The suggested coordination mode in the oxidovanadium(IV) complex interpreted by FTIR
465 (Experimental and theoretical), diffuse reflectance and UV/Vis spectroscopy, and
466 supported by the theoretical analysis was also substantiated by EPR measurements.

467 The X-band EPR powder spectrum of the [VOL₂H₂O] complex, recorded at room
468 temperature, is shown in Figure 4A. The main feature is a broad and isotropic signal with a
469 g_0 value of 1.961 which is in concordance with a nearly axial ligand field as is usually
470 observed for vanadium complexes owing vanadium-oxygen interactions (O-V-O) in the
471 oxidovanadium(IV) unit.³² Some weaker signals are also observed superposed on the
472 central line; they correspond to the hyperfine structure of a V(IV) isolated species (100%
473 abundant ⁵¹V nucleus with $I = 7/2$).

474 In order to establish the binding mode of the ligand and to identify the bioactive
475 solution species of the [VOL₂H₂O] complex, EPR studies of the dissolved powder were
476 performed. Figure 4B, shows the signal obtained in a DMF solution, at 298 K. The EPR
477 signal shows the typical eight-line pattern spectrum for the oxidovanadium(IV) cation
478 systems indicating the formation of single mononuclear species after the dissolution
479 process. The spectral simulation, by the Bruker Simfonia program, predicted the formation
480 of an oxidovanadium(IV) chromophore with spin Hamiltonian parameters of $g_0 = 1.988$
481 and $A_0 = 108.3$ G (100.5×10^{-4} cm⁻¹). This signal is coincident with the formation of
482 oxidovanadium(IV) complexes with oxygen containing ligands and solvation at the *cis*-

1
2
3 483 position in which the isotropic hyperfine coupling constant is larger than that obtained for
4
5 484 the *trans*- isomer.³³ The reduction of the hyperfine splitting constant value (A_0) and the
6
7 485 increment of the g_0 parameter is expected, in comparison with those to the
8
9 486 oxidovanadium(IV) free cation ($V(IV)O^{2+}$, $g_0 = 1.964$ and $A_0 = 106.3 \times 10^{-4} \text{ cm}^{-1}$),³⁴ when
10
11 487 negatively charged carboxylate groups are in the first coordination sphere.
12
13
14

15 488

16 489 **3.4. Biological activities**

17 490 **3.4.1. Acid (AcP) and alkaline (ALP) phosphatase inhibition assays**

18 491

19 492 As mentioned above, researchers are excited in the development of chemotherapeutic
20 493 agents.³⁵ Simple salts and several vanadium(IV) and (V) complexes have demonstrated
21 494 inhibition abilities against phosphatases.³⁶ Based on this assumption, the inhibition ability
22 495 of the peroxidovanadium(V) and oxidovanadium(IV) complexes were determined.

23 496 In both assays, the activity of the free ligand, oxidovanadium(IV) sulfate and
24 497 peroxidovanadium(V) species was also assessed. In Figure 5A it can be observed the AcP
25 498 inhibition experiments. The free ligand had no inhibitory effect on AcP. The
26 499 peroxidovanadium(V) complex did not inhibit phosphatase activity and its activity
27 500 remained almost constant up to the higher tested concentrations (100-500 μM). On the
28 501 other hand, the oxidovanadium(IV) complex inhibits the enzymatic activity. It was less
29 502 efficient than the oxidovanadium(IV) sulfate, resulting in a 50% of inhibition of the
30 503 activity at a concentration of 250 μM (IC_{50}).

31 504 The data in Figure 5B showed the inhibitory effects of the compounds on the ALP
32 505 at various concentrations. The ligand 4-aminobenzoic acid, the peroxidovanadium(V)
33 506 species and the oxidovanadium(IV) complex showed no significant inhibition.

1
2
3 507 Surprisingly, the peroxidovanadium(V) complex exerted better inhibition than the
4
5 508 oxidovanadium(IV) sulfate salt from concentrations higher than 50 μM reaching at a 50%
6
7
8 509 of inactivation of the enzyme at 500 μM concentration value.

9
10
11 510 Amino derivative vanadium complexes demonstrated specific activity against
12
13 511 phosphatases. The studied oxidovanadium(IV) complex behaves as a better inhibitor
14
15 512 toward acid phosphatase, whereas peroxidovanadium(V) complex has superior inhibition
16
17 513 effect on ALP.

18
19
20 514 It would be possible to find tentative explanations for these behaviors based on the
21
22 515 following considerations. In a previous work, McLauchlan *et al*³⁶ performed a series of
23
24 516 inhibition experiments on alkaline phosphatase (bovine calf intestine) and acid phosphatase
25
26 517 (wheat germ) employing vanadium complexes containing the bidentate ligand picolinate
27
28 518 and the metal in (III), (IV) and (V) oxidation states. They concluded about the relevance of
29
30 519 the oxidation state and provided evidence that, in general, the most effective inhibitors are
31
32 520 the complexes with an oxidation state of (V). Thus, one of the factors involved in the
33
34 521 difference in the effect on ALP of $[\text{VOL}_2\text{H}_2\text{O}]$ and $[\text{VO}(\text{O}_2)\text{L}(\text{H}_2\text{O})]\cdot\text{H}_2\text{O}$ complexes could
35
36 522 possibly be associated to the oxidation state of vanadium. Indeed, it was proposed that for
37
38 523 the alkaline phosphatase the complexes containing vanadium are more efficient in an
39
40 524 oxidation state of (V).³⁷

41
42
43 525 It might also be thought that the optimum pH values for enzymatic action could be
44
45 526 related to these differences in their activity. It is well known that oxidovanadium(IV)
46
47 527 species are more stable close to neutral pH range in opposition to the effect of
48
49 528 vanadium(V) species.³⁸

50
51
52 529 Electronic nature of ancillary ligands is another factor that could be taken in
53
54 530 consideration in the physiological effects of vanadium complexes. In experiments of
55
56
57
58
59
60

531 cytotoxicity on Rat hepatoma H4IIEC3 cells, a series of peroxidovanadium(V) complexes
532 with pentagonal-bipyramidal structure have been tested.³⁹ It has been found that the IC₅₀
533 values are greater than those produced by a 1:1 mixture of hydrogen peroxide and sodium
534 orthovanadate and concluded that the incorporation of organic ligand moderates the
535 cytotoxicity of vanadium, and that the electronic properties of the peroxy group affected
536 the physiological activity of the complexes. Ziegler *et al.* studied the inhibition potency of
537 a series of systematically modified oxidovanadium(IV)- β -diketone complexes.⁴⁰ They
538 analyzed the inhibitory potency on calf-intestine alkaline phosphatase and correlated the
539 calculated charge on VO unity with the effect of each metal complex. Their conclusion
540 supports the idea that a more positive center led to the complex more tightly bound to the
541 enzyme, and consequently behaving as a stronger inhibitor agent. If we assume this
542 possibility and evaluate the calculated Mulliken charge on the VO group for [VOL₂H₂O],
543 and compare the data with that calculated for the [VO(O₂)L(H₂O)]·H₂O complex, these
544 values are 0.50 and 0.64 (a.u.), respectively. Then, it can be proposed that
545 peroxidovanadium(V) complex acts as a more positive center than oxidovanadium(IV)
546 complex against ALP. Considering as well as the others factors, it can be assumed for
547 neutral complexes that electron density on vanadium ion affects the enzyme interaction or
548 the membrane transport.

549 In summary, the prevalence of oxidation state, the coordination number that
550 complex adopts in solution, the pH and the electron density on VO group do possibly
551 affect significantly their activities. We cannot discard others factors involved as the type of
552 interaction, mechanism of inhibition, stability, etc., but further studies are needed to
553 elucidate them.

554 It can also be mentioned that VO(O₂)⁺ species was able to inhibit in a stronger
555 manner the acid phosphatase (potato source), contrary to its effect on the acid phosphatase

1
2
3 556 from wheat germ (Figure 5A).⁴¹ Furthermore, it is evident that peroxidovanadium(V)
4
5 557 complex did not inhibit AcP. There is not so much information about inhibitory power of
6
7 558 peroxidovanadium complexes, but potent inhibition on AcP has been related to the greater
8
9 559 affinity of the inhibitors for imidazole nitrogen of the enzyme. Nevertheless, acid
10
11 560 phosphatases from different sources may provide different inhibitions capacity for the
12
13 561 same vanadium compound.⁴²

14
15
16
17 562 Some aspects revealed in this work can be discussed in association with other
18
19 563 previous reported vanadium-based phosphatase inhibitors (Table 3). To provide a
20
21 564 comparative analysis, the presences of free NH groups as well as the influence of the
22
23 565 phenyl group as part of the ligand were considered. Phenyl moiety was selected to explore
24
25 566 if such types of compounds would be more portent inhibitors considering their structural
26
27 567 relationship with phenol and the PNPP substrate. The formation of vanadate phenyl ester,
28
29 568 produced an improvement of the inhibition ability of vanadate alone.^{43,44} According to these
30
31 569 studies, vanadate in presence of phenol significantly improved the inhibition potency on *E.*
32
33 570 *coli* alkaline phosphatase due to the formation of species analogous to organic phosphate
34
35 571 esters.⁴⁴

36
37
38
39 572 The results of McLauchlan *et al*³⁶ demonstrated that, in the case of vanadium
40
41 573 complexes containing the ligand imidazole-4-carboxylate (imc), the values for the
42
43 574 Michaelis binding constant (K_m) showed that VO(imc)₂ complex had the lower $K_m = 3.3$
44
45 575 μM value denoting stronger affinity for wheat germ acid phosphatase and, the greater
46
47 576 K_m values were for ALP and PTP1B in opposition to the data observed for the VO₂(imc)₂⁻
48
49 577 (Table 3). This affinity is comparable in some way to the results obtained in this work
50
51 578 where the oxidovanadium(IV) complex behaved as a better inhibitor of the AcP and the
52
53 579 peroxidovanadium(V) complex of the ALP. The anthranilate (2-aminobenzoate) vanadium
54
55 580 complexes (VO(anc)₂, VO₂(anc)₂⁻) worked in a similar way for PTP1B but not for AcP.

1
2
3 581 These results are possible due to the lack of the free NH groups because contrasting
4
5 582 aminobenzoate vanadium complexes they are involved in the coordination to the metal
6
7 583 center. Structurally similar complexes with phenyl derivative ligands were VO(trop)₂ and
8
9 584 VO(hino)₂⁴⁵ (Table 3). Both were tested on PTP1B denoting higher inhibition activity for
10
11 585 the VO(hino)₂ complex. The difference between the ligands is that the hino ligand has an
12
13 586 additional –CH₂(CH₃)₂ group attached to the benzoic moiety. This structural modification
14
15 587 causes the reduction in 50 % of the IC₅₀ value. VO(imc)₂ and VO(hino)₂ complexes could
16
17 588 also be compared. Regardless the differences of the experimental method, K_m value for
18
19 589 VO(hino)₂ is significantly lower (0.15 μM) than for VO(imc)₂ (43 μM). The hypothesis
20
21 590 concerning to the vanadium delivery to the active site of the enzyme could be the
22
23 591 explanation of the inhibition ability of VO(hino)₂. Possibly, the VO₄ coordination sphere
24
25 592 was more favorable for vanadate formation.^{4,12,36,44} Ligand selectivity is also observed
26
27 593 when biguanide oxidovanadium(IV) complexes ([VO(Big)₂].H₂O, [VO(Big1)₂].2H₂O)
28
29 594 were compared.⁴⁶ The oxidovanadium complex that contain the phenyl group as part of the
30
31 595 ligand acted as a better inhibitor on ALP than on PTP1B. Another example arises from the
32
33 596 comparison between dioxidovanadium(V) complexes [VO₂(L¹)₂](Et)₃NH]₂ (L¹= 2,4-
34
35 597 (dihydroxyphenyl)ethylidene)benzohydrazide) and [VO₂(L²)₂](DBU-H)₂ (L² = bis[(3-
36
37 598 hydroxy-5-(hydroxymethyl)-2-methylpyridin-4-yl)methylene]oxalohydrazide).⁴⁷The
38
39 599 complex having L¹ ligand was an efficient PTP1B inhibitor (Table 3).

40
41
42
43
44
45
46
47 600 As it was stated, there is scarce information related to inhibition ability on AcP,
48
49 601 ALP or PTPB1 of peroxidovanadium(V) complexes having a structurally related ligand to
50
51 602 4-aminobenzoate anion. However, the following examples can be considered. Water-
52
53 603 soluble polymer matrices containing bis-peroxo vanadium complexes
54
55 604 ([VO(O₂)₂(sulfonate)]-PSS, [V₂O₂(O₂)₄-(carboxylate)-VO(O₂)₂(sulfonate)]-PSSM) have
56
57 605 been proved on ALP and contrasted with Na[VO(O₂)₂(H₂O)] (Table 3).⁴⁸ The
58
59

606 bisperoxidovanadium(V) polymeric complexes were more effective than the
607 peroxidovanadium(V) vanadium complex ($[\text{VO}(\text{O}_2)\text{L}(\text{H}_2\text{O})]$). Interestingly, the peroxide
608 species ($[\text{VO}(\text{O}_2)]^+$) did not inhibit intestinal ALP whereas the bisperoxide showed
609 inhibitory activity ($\text{IC}_{50}=25.18 \mu\text{M}$). This marked difference in reactivity may be possibly
610 associated to the aqueous stability of perovanadates.⁴⁹

611 Finally, the peroxido complexes $[\text{VO}(\text{O}_2)\text{L}(\text{H}_2\text{O})]\cdot\text{H}_2\text{O}$ (L=4-aminobenzoate) and
612 $\text{NH}_4[\text{VO}(\text{O}_2)(\text{dipic})(\text{H}_2\text{O})]^{50}$ have acted as ALP inhibitors (Table 3). As it was shown, in
613 $[\text{VO}(\text{O}_2)\text{L}(\text{H}_2\text{O})]\cdot\text{H}_2\text{O}$ the vanadium center is located in a pentagonal pyramid with a
614 bidentate coordination mode of the peroxo and the carboxylate group including a water
615 molecule in the equatorial position. In $\text{NH}_4[\text{VO}(\text{O}_2)(\text{dipic})(\text{H}_2\text{O})]$ complex the vanadium
616 atom environment is a seven-coordinate distorted pentagonal bipyramid with the vanadyl
617 oxygen and the water molecule at the apices and the peroxo group, nitrogen and two
618 monodentate carboxylate groups in the pentagonal plane. It can be assumed that in solution
619 the $[\text{VO}(\text{O}_2)\text{L}(\text{H}_2\text{O})]\cdot\text{H}_2\text{O}$ complex may adopt a seven coordinate structure similar to
620 $\text{NH}_4[\text{VO}(\text{O}_2)(\text{dipic})(\text{H}_2\text{O})]$ thus it could be suggested that this type of structural
621 arrangement around vanadium(V) tends to favor enzyme inhibition.

622

623 3.4.42. Analysis of the inhibitory effect by FTIR spectroscopy

624 (i) Substrate (*p*-nitrophenylphosphate) bands

625

626 The inhibition or the stimulation effect can be clearly seen by studying the FTIR changes
627 in the finger print region ($1230\text{-}840 \text{ cm}^{-1}$) of the substrate (*p*-nitrophenylphosphate)
628 corresponding to the phosphate group vibrations upon enzymatic or non-enzymatic
629 hydrolysis.⁵¹

1
2
3 630 Lyophilized blank solution containing all the reactants, except ALP enzyme
4
5 631 showed the presence of the typical phosphate bands: 1115 cm⁻¹, 1043 cm⁻¹ and 981 cm⁻¹ ⁵²
6
7 632 (Figure 6). There was a drastic lowering in the 1115 cm⁻¹ band intensity (50%) as a
8
9 633 consequence of the ALP action on the phosphate hydrolysis. When the 4-aminobenzoic
10
11 634 acid or the oxidovanadium(IV) complex were included in the reaction media, there was no
12
13 635 significant changes in the intensity of the main band of the substrate observed at 1115 cm⁻¹
14
15 636 with respect to the control with ALP. There is some decrease in the intensity of the 980 cm⁻¹
16
17 637 band that may imply some kind of interaction between the phosphate group and those
18
19 638 compounds. Besides, no interference with the corresponding bands of $\nu(\text{V}=\text{O})$ stretching
20
21 639 frequencies of the oxidovanadium(IV) (965 cm⁻¹) and peroxidovanadium(V) (998 cm⁻¹)
22
23 640 complexes has been observed, due to the low concentration of the complexes. In
24
25 641 opposition, in the presence of the peroxidovanadium(V) complex, the spectrum showed
26
27 642 that the intensity of the band related to the phosphate group did not significantly decrease
28
29 643 in comparison with the spectrum of the blank, suggesting lack of the phosphate hydrolysis
30
31 644 process in concordance with the inhibition effect.

32
33 645 Unfortunately in the case of the AcP, the obtained FTIR spectra did not passed the
34
35 646 quality test in order to be analyzed.

36
37 647

38 39 648 **(ii) Conformational changes in the secondary structure of phosphatase enzymes**

40
41 649

42
43
44
45
46 650 There are some studies that use FTIR spectroscopy to analyze the conformational
47
48 651 changes that occur on the secondary structure of the phosphatases under different type of
49
50 652 conditions as hyperbaric manipulation⁵³, thermal and pH modifications⁵⁴, interaction with
51
52 653 some metal ions⁵⁵ or with tartaric acid.⁵⁶ It was known that the main spectral features of
53
54
55
56
57
58
59
60

1
2
3 654 both enzymes are the characteristic strong Amide I band located at c.a. $\sim 1658\text{ cm}^{-1}$ which
4
5 655 is indicative of the predominance of the α -helix conformation on the secondary
6
7 656 structure.^{55,56} It is also well established that an attachment of any compound to the enzyme
8
9 657 is able to produce conformational changes that can be observed by FTIR spectroscopy
10
11 658 analyzing the different components of the Amide I band. In this section, a quantitative
12
13 659 analysis of each conformational component such as α -helix, β -sheet, turns, solvate helix
14
15 660 and random coil structures is provided in order to get a deeper insight about the possible
16
17 661 modifications that the inhibitors provoke on enzyme structure.

18
19 662 As it can be seen from Table 4, the curve-fitting procedure based on the second
20
21 663 derivative spectra indicated that the α -helix content of the ALP control sample is about
22
23 664 39.59%. The interaction of oxidovanadium(IV) complex and 4-aminobenzoic acid (non-
24
25 665 inhibitors) did not produced remarkable changes on the Amide I components. The α -helix
26
27 666 conformation slightly decreased ($\sim 13\text{-}14\%$) whereas the most remarkable change is the
28
29 667 increment in percentage of the β -antiparallel structure. The observed losses of the
30
31 668 percentages of α -helix native structure, accompanied by the increment of the β -antiparallel
32
33 669 structure did not affect in a great extent the main conformation of the enzyme. This is
34
35 670 consistent with the maintenance of the structure integrity of the ALP enzyme and its
36
37 671 activity as a consequence. On the contrary, a drastic reduction in the α -helix conformation
38
39 672 ($\sim 40\%$) was observed for the compounds that produced inhibition on the ALP activity
40
41 673 (peroxidovanadium(V) complex). This loss of the α -helix (un-solvated) conformation was
42
43 674 cooperative with the gain of solvated α -helix structure. Those changes can be explained in
44
45 675 terms of the solvent accessibility. The native α -helix ($1650\text{-}1658\text{ cm}^{-1}$) is shown to be
46
47 676 protected from the solvent by a tertiary fold. However, in the absence of this protection the
48
49 677 helix become solvated and a spectral band at c.a. $\sim 1630\text{ cm}^{-1}$ appeared in the FTIR
50
51
52
53
54
55
56
57
58
59
60

1
2
3 678 spectrum.^{57,58} It is then suggested that under the presence of inhibitors, the secondary
4 structure of ALP became more flexible and more exposed. As a result, ALP allows the
5 679 structure of ALP became more flexible and more exposed. As a result, ALP allows the
6 structure of ALP became more flexible and more exposed. As a result, ALP allows the
7 680 compounds to interact producing structural changes that block its activity. There was no
8 presence of random coil structure component (1637-1645 cm⁻¹) in the ALP analyzed
9 681 presence of random coil structure component (1637-1645 cm⁻¹) in the ALP analyzed
10 682 samples.
11
12
13

14
15 683 In the case of the AcP inhibitor, the oxidovanadium(IV) complex (Table 4), a
16 rearrangement involving a lowering in the percentage contribution of α -helix and random
17 684 rearrangement involving a lowering in the percentage contribution of α -helix and random
18 coil structures, and a remarkable increment in the percentage of the solvated helix structure
19 685 coil structures, and a remarkable increment in the percentage of the solvated helix structure
20 were produced. Again, the solvent accessibility could be involved but there was an
21 686 were produced. Again, the solvent accessibility could be involved but there was an
22 additional structural modification: a decrease of 20% in the percentage of the random coil
23 687 additional structural modification: a decrease of 20% in the percentage of the random coil
24 component that could led to AcP activity inhibition.
25 688 component that could led to AcP activity inhibition.
26
27
28
29
30
31
32
33
34
35
36
37
38
39
40
41
42
43
44
45
46
47
48
49
50
51
52
53
54
55
56
57
58
59
60

690 4. Albumin interactions

691
692 Because serum albumin is one of the most abundant transporter-protein in plasma, the
693 affinity of drugs towards albumin can be correlated with a better accessibility to the target.
694 Albumin plays an essential role in the increment of solubility and in the cellular delivery of
695 compounds present in blood. For that reason the study of the interaction of selected
696 compounds with the protein have significance in the binding properties of the complexes.
697 Fluorescence quenching experiments were performed for the peroxidovanadium(V)
698 complex. The intensity of the complex band was negligible with respect to the band
699 corresponding to its interaction with albumin. A decrease in the albumin fluorescence
700 intensity was observed when measurements were performed at fixed BSA concentration (6
701 μ M) and increasing concentrations of the peroxidovanadium(V) complex varying from 1 to

1
2
3 702 100 μM . The fluorescence quenching data were analyzed by the Stern-Volmer equation
4
5 703 The plot F^0/F vs $[Q]$ showed a positive deviation indicating the presence of both static and
6
7 704 dynamic quenching⁵⁹ by the same fluorophore (Figure 7, left). Assuming one type of
8
9 705 quenching process at lower concentrations, K_{sv} constant were evaluated at the two
10
11 706 temperatures (Figure 7, left, inset) and the calculated values were $K_{sv} = 3.92 \times 10^4 \text{ M}^{-1}$
12
13 707 (298K) and $K_{sv} = 3.58 \times 10^4 \text{ M}^{-1}$ (310K). In addition, the quenching rate constant K_q could
14
15 708 be estimated through the relationship $K_q = K_{sv}/\tau_0$ (τ_0 = average lifetime of the biomolecule
16
17 709 without quencher assumed to be 10^{-8} s for the fluorescence lifetime of the biopolymer).
18
19 710 Then, both estimated K_q values $3.92 \times 10^{12} \text{ M}^{-1} \cdot \text{s}^{-1}$ (298K) and $K_{sv} = 3.58 \times 10^{12} \text{ M}^{-1} \cdot \text{s}^{-1}$
20
21 711 (310K) resulted higher than the maximum scatter collision quenching constant of various
22
23 712 quenchers with the biopolymer ($2 \times 10^{10} \text{ M}^{-1} \cdot \text{s}^{-1}$).⁴⁷ Consequently, static type of quenching
24
25 713 can be assumed involving a compound formation between the complex and BSA.
26
27 714 Furthermore, from the plot $\log[(F^0-F)/F]$ versus $\log[Q]$ (Figure 7, right), the binding
28
29 715 constants and the number of binding sites, were calculated being $K_b = 2.29 \pm 0.01 \times 10^5 \text{ M}^{-1}$
30
31 716 (298K) and $K_b = 1.82 \pm 0.01 \times 10^5 \text{ M}^{-1}$ (303K), and $n \sim 1$ at both temperatures. It is well
32
33 717 acknowledged that reversible binding to one high-affinity sites of the albumin is
34
35 718 accompanied by association constant (K_b) values from 10^4 to 10^6 M^{-1} indicating a carrier-
36
37 719 like behavior.⁶⁰ Thus, the K_b values of the complex suggested that it could be transported
38
39 720 by BSA and that there were no significant differences in the binding ability at both
40
41 721 temperatures. In addition, the value of $n \sim 1$ suggested that there is almost one class of
42
43 722 binding site to peroxidovanadium(V) complex at BSA. Finally, to analyze the acting forces
44
45 723 between the complex and albumin, thermodynamic parameters were evaluated, in which
46
47 724 $\Delta G^\circ = -30.56 \text{ KJ/mol}$, $\Delta H^\circ = 14.69 \text{ KJ/mol}$ and $\Delta S^\circ = 151.84 \text{ J/K.mol}$. The negative value of
48
49 725 ΔG° indicates that the interaction of the complex with BSA is spontaneous and the driving
50
51 726 force is mainly an entropic factor. The values of both ΔH° and ΔS° are positive, which

727 suggested that the main contribution to these changes arise from hydrophobic
728 interactions.⁶¹

729 Due to the interference of 4-aminobenzoic acid and oxidovanadium(IV) complex in
730 the fluorescence quenching experiments, their interaction with BSA was studied examining
731 UV/Vis and 3D fluorescence spectra.

732 UV/Vis spectroscopy is a simple method to investigate structural changes in BSA
733 and determine complex formation. BSA shows a characteristic UV/Vis spectrum with two
734 bands located at c.a. 220 and 280 nm. The band at higher energy can be correlated to
735 $n \rightarrow \pi^*$ transition of C=O in the backbone of the protein (peptide bonds) and the band at
736 lower energy comes from the amino acid side chains (phenyl rings in Trp, Tyr and Phe
737 residues) and both are sensitive to conformational changes.⁶²

738 UV/Vis absorption measurements are shown in Figure 8. In the system ligand-BSA
739 (Figure 8, A), increasing concentrations of the ligand lead to an increase and a shift to
740 lower wavenumber of the BSA band located at 280 nm. This change can be attributed to
741 the contribution of the band belonging to the ligand (263 nm). Indeed, a comparison of the
742 ligand spectrum (20 μ M) mixed with BSA (6 μ M) showed the presence of two bands
743 located at 268 and 283 nm in which the band belonging to BSA slightly its intensity
744 (Figure 8 A, inset). For the complex, the interaction seems to be different. The complex did
745 not show the band at \sim 280 nm (Figure 8 C). The BSA band increased its intensity in
746 contact with the complex and there was no significant change in the maximum at \sim 280 nm
747 (Figure 8 B). These behaviors correlated with hydrophobic type of interaction that may
748 possible happen, due to a $\pi \rightarrow \pi$ stacking between aromatic ring of the complex and the
749 phenyl rings of aromatic aminoacids residues in the protein. In addition, the band at 220
750 nm slightly moved to higher wavelength suggesting changes in the polypeptide chain of
751 BSA (Figure 8 B).

1
2
3 752 Additional information can be obtained from the 3D fluorescence spectroscopy spectra
4
5 753 Peak 1 is the Rayleigh scattering peak ($\lambda_{ex} = \lambda_{em}$). Peak A ($\lambda_{ex} = 280$ nm, $\lambda_{em} = 337.9$
6
7 754 nm) is representative of Trp and Tyr residues, and the fluorescence intensity of the residues
8
9 755 related with the polarity of the microenvironment (Figure 9A). Peak B ($\lambda_{ex} = 230$ nm,
10
11 756 $\lambda_{em} = 340.7$ nm) is associated to the polypeptide backbone structure. As can be seen from
12
13 757 Figures 9B and 9C, and Table 5, Peak A increased its intensity for the ligand and the
14
15 758 complex, in comparison to BSA. Although quenching behavior is usually expected,
16
17 759 sometimes the increment of fluorescence intensity occurs and is suggested to be due the
18
19 760 increase of the quantum efficiency of the compound. This behavior has been previously
20
21 761 observed and associated to an intercalative action of the ligands and complexes with NH
22
23 762 groups.⁶³ It can be noted that the ligand 4-amino benzoic acid increased the intensity of
24
25 763 Peak A more strongly than the complex.

26
27 764 The most remarkable change was observed for Peak B (Table 5). In the presence of the
28
29 765 oxidovanadium(IV) complex this peak practically disappeared, in contrast to the ligand
30
31 766 which intensity increased once more. The decrease of the band produced by the complex
32
33 767 has been associated with changes in the peptide strands (unfolding). This causes the
34
35 768 exposition of hydrophobic regions, together with a lowering of the α -helix content as a
36
37 769 result of the impact of the interaction.⁶⁴ Thus, different kind of interactions were produced
38
39 770 by the ligand and the complex, in agreement with the different observations in the UV/Vis
40
41 771 spectra.

772

773 5. Conclusions

774

775 New oxidovanadium complexes containing vanadium(V) ($[\text{VO}(\text{O}_2)\text{L}(\text{H}_2\text{O})] \cdot \text{H}_2\text{O}$) and (IV)
776 ($[\text{VOL}_2\text{H}_2\text{O}]$) have been synthesized. The vanadium centers are both coordinated to 4-

1
2
3 777 aminobenzoic in a bidentate mode through carboxylate group. The proposed structures
4
5 778 were supported by computational data analysis based in DFT theory. For the
6
7 779 oxidovanadium(IV) complex a *cis*-conformation was assumed in concordance with FTIR,
8
9 780 UV/Vis and EPR spectroscopies. Related to the biological *in vitro* assays, the amino
10
11 781 derivatives complexes behaved in a selective way with respect to the phosphatases
12
13 782 inhibition: $[\text{VO}_2\text{L}_2\text{H}_2\text{O}]$ inhibited AcP, while $[\text{VO}(\text{O}_2)\text{L}(\text{H}_2\text{O})]\cdot\text{H}_2\text{O}$ inhibited ALP. This
14
15 783 inhibitory behavior was contrasted using FTIR spectroscopy demonstrating that in the
16
17 784 presence of peroxidovanadium(V) complex ALP was not able to hydrolyze phosphate
18
19 785 group belonging to the *p*-NPP and that action may be due to the strong loss of the α -helix
20
21 786 conformation (~40%) in the Amide I band. In this work we focused the study in the
22
23 787 chemistry of the complexes, their ability to inhibit ALP or AcP and followed the inhibition
24
25 788 action by using FTIR spectroscopy. However, further studies are needed to elucidate the
26
27 789 mechanism, type of inhibition and stability. Albumin interaction was investigated for the
28
29 790 ligand and both complexes. Peroxidovanadium(V) complex produced a quenching effect
30
31 791 on the fluorescence spectrum of BSA and their binding constant value denoted a static
32
33 792 quenching process. Both the ligand and the oxidovanadium(IV) complex produced an
34
35 793 enhancement of its fluorescence intensity after albumin interaction and the changes were
36
37 794 evaluated through 3D fluorescence experiments which showed a more drastic
38
39 795 rearrangement for the metal complex, because of the disappearance of Peak B, associated
40
41 796 to the protein polypeptide backbone structure.
42
43
44
45
46
47
48
49
50
51

52 798 **Conflicts of interest**

53
54
55 799 There are no conflicts to declare.
56
57
58
59
60

1
2
3 801 **Electronic Supplementary Information. Figure S1.** Structure and selected bond lengths
4 (Å) and angles (°) for *trans*-[VOL₂H₂O] complex. **Figure S2.** FTIR spectra of 4-
5 802 aminobenzoic acid, sodium aminobenzoate, [VOL₂H₂O] and [VO(O₂)L(H₂O)].H₂O.
6 803 **Figure S3.** Calculated bands in the UV-vis spectra of [VO(O₂)L(H₂O)].H₂O. **Figure S4.**
7 804 Calculated bands in the UV-vis spectra of [VOL₂H₂O]. **Figure S5, S6 and S7.** Contour
8 805 spectra and three-dimensional fluorescence spectra of 6 μM BSA, 6 μM BSA-20 μM 4-
9 806 aminobenzoic acid and 6 μM BSA-20 μM [VOL₂H₂O], respectively.
10 807
11 808

809 Acknowledgments

810 This work was supported by Consejo Nacional de Investigaciones Científicas y Técnicas
811 (CONICET, PIP 0611), Agencia Nacional de Promoción Científica y Tecnológica
812 (ANPCyT, PICT16-1814), Universidad Nacional de La Plata (UNLP, X777) of Argentina.
813 LGN and EGF are Research Fellows of CONICET. JEP and PAMW are Research Fellows
814 of Comisión de Investigaciones Científicas de la Provincia de Buenos Aires (CICPBA)
815 Argentina.
816

818 **Abbreviations**

819

[VO(O ₂)L(H ₂ O)].H ₂ O	[VO(O ₂)(C ₇ H ₆ NO ₂)(H ₂ O)].H ₂ O
[VOL ₂ H ₂ O]	[VO(C ₇ H ₆ NO ₂) ₂ H ₂ O]
AcP	Acid phosphatase
ALP	Alkaline phosphatase
BSA	Bovine serum albumin
DMF	Dimethylformamide
DMSO	Dimethyl sulfoxide
p-NPP	Paranitrophenyl phosphate
Tris-HCl	Tris(hydroxymethyl)aminomethane hydrochloride

820

821

823 **Figures**View Article Online
DOI: 10.1039/C9NJ01638D

824

825 **Figure 1.** Optimized geometry at the level of theory B3LYP/6-311+g* of oxidovanadium
826 complexes: [VO(O₂)L(H₂O)].H₂O (A, left) and *cis*-[VOL₂H₂O] (B, right).

827

828 **Figure 2.** [VO(O₂)L(H₂O)].H₂O complex: **(A)** **(a)** Diffuse reflectance spectrum in the 220-
829 550 nm region, **(b)** peak fitting procedure with contribution of three involved bands; **(B)**
830 **(a)** Electronic absorption spectra in the 260-600 nm region (2.7 x 10⁻³M, DMF), **(b)**
831 calculated spectrum, **(c)** peak fitting procedure with contribution of three involved bands.

832

833 **Figure 3.** [VOL₂H₂O] complex: **(A)** Diffuse reflectance spectrum in the 220-850 nm
834 region, **(B)** Electronic absorption spectra in the 425-890 nm region (0.11 M, DMF), **(C)**
835 Calculated *cis* and *trans* spectra.

836

837 **Figure 4.** **(A)** Powder EPR spectrum of [VOL₂H₂O] obtained at 77 K, frequency 9.42
838 GHz; **(B)** Sample dissolved in DMF, at room temperature, in quartz flat cell, frequency
839 9.70 GHz.

840

841 **Figure 5.** Effect of 4-aminobenzoic acid (▼), VOSO₄.5H₂O (■), [VO(O₂)L(H₂O)].H₂O
842 (▲), [VO(O₂)]⁺ (◆) and [VOL₂H₂O] (●) on **(A)** on AcP activity and **(B)** ALP activity. The
843 values are expressed as the mean ± SEM of at least three independent experiments.
844 *significant values in comparison with the basal level (p < 0.05)

845

1
2
3 846 **Figure 6.** FTIR changes in the finger print region ($1230\text{-}840\text{ cm}^{-1}$) of the substrate PNPP New Article Online
DOI: 10.1039/C9NJ01638D
4 (4-nitrophenylphosphate): Liophilized blank solution containing all the reactant except
5 847 (4-nitrophenylphosphate): Liophilized blank solution containing all the reactant except
6 ALP enzyme (solid line); liophilized blank solution containing all reactants including
7 848 ALP enzyme (Dash line); all the reactant + $[\text{VO}(\text{O}_2)\text{L}(\text{H}_2\text{O})]\cdot\text{H}_2\text{O}$ (■), all the reactant +
8 849 $[\text{VOL}_2\text{H}_2\text{O}]$ (●) ; all the reactant + 4-aminobenzoic acid (L, ▲).
9
10
11
12
13
14

15 851
16
17
18 852 **Figure 7.** $[\text{VO}(\text{O}_2)\text{L}(\text{H}_2\text{O})]\cdot\text{H}_2\text{O}$: left: Stern-Volmer plot F^0/F vs $[Q]$, right: Plot of log
19 853 $[(F^0-F)/F]$ vs log $[Q]$.
20
21
22
23
24

25 854
26 855 **Figure 8.** UV-Vis spectra in the 220-300 nm region: (A) 4-aminobenzoic acid-BSA system
27 856 (inset: deconvolution of the ~ 280 nm band), (B): $[\text{VOL}_2\text{H}_2\text{O}]$ -BSA system (6 μM BSA,
28 857 increasing concentrations of ligand and complex from 0-60 μM), (C): solid line: 6 μM
29 858 BSA, short dash: 6 μM BSA-20 μM aminobenzoic acid, gray line: 20 μM 4-aminobenzoic
30 859 acid, dotted line: 6 μM BSA-20 μM $[\text{VOL}_2\text{H}_2\text{O}]$, dash dot line: 20 μM $[\text{VOL}_2\text{H}_2\text{O}]$.
31
32
33
34
35
36
37
38
39
40

41 860
42 861 **Figure 9.** Three-dimensional fluorescence spectra of 6 μM BSA, 6 μM BSA-20 μM 4-
43 862 aminobenzoic acid and 6 μM BSA-20 μM $[\text{VOL}_2\text{H}_2\text{O}]$.
44
45
46
47
48
49
50
51
52
53
54
55
56
57
58
59
60

869 **References**View Article Online
DOI: 10.1039/C9NJ01638D

870

871 [1] K.H. Thompson and C. Orvig, *Dalton Trans.*, 2006, 761.

872

873 [2]. D.C. Crans and T.J. Meade, *Inorg. Chem.* 2013, **52**, 12181.

874

875 [3]. J. Costa Pessoa, S. Etcheverry and D. Gambino, *Coord. Chem. Rev.* 2015, **301–302**,
876 24.

877

878 [4]. D.C. Crans, L. Yang, A. Haase and X. Yang, *Met. Ions Life Sci.* 2018, **18**, 251.

879

880 [5] M. Sutradhar, L.M.D.R.S. Martins, M.F.C. Guedes da Silva and A.J.L. Pombeiro,
881 *Coord Chem Rev.* 2015, **301-302**, 200.

882

883 [6] G. Süss-Fink, S. Stanislas, G.B. Shul'pin, G.V. Nizova, H. Stoeckli-Evans, A. Neels, C.
884 Bobillier and S. Claude. *J. Chem. Soc., Dalton Trans.*, 1999, 3169.

885

886 [7] G.R. Willsky, L-H Chia, M. Godzala III, P.J. Kostyniaka, J.J. Smeed, A.M. Trujillo,
887 J.A. Alfano, W. Ding, Z. Huc and D.C. Crans. *Coord. Chem. Rev.* 2011, **255**, 2258.

888

889 [8] T. Koleša-Dobravc, K. Maejima, Y. Yoshikawa, A. Meden, H. Yasui and F. Perdih.
890 *New J. Chem.*, 2018, **42**, 3619.

891

892 [9]. H. Cho, *Vitam. Horm.* 2013, **91**,405.

893

894 [10] M. al-Rashida1 and J. Iqbal, *Mini-Rev. Med. Chem.*, 2015, **15**, 41.

- 1
2
3 895 [11] N. Alimoradi, M.R. Ashrafi-Kooshk, M. Shahlaei, S. Maghsoudi, H. Adibi, R.P. New Article Online
DOI: 10.1039/C9NJ01638D
- 4
5 896 McGeary and R. Khodarahmi, *J. Enz. Inhib. Med. Chem.* 2017, **32**, 20.
- 6
7 897
- 8
9 898 [12]. C. C. McLauchlan, B.J. Peters, G.R. Willsky and D.C. Crans, *Coord. Chem. Rev.*
- 10 899 2015, **301–302**, 163.
- 11
12 900
- 13
14 901 [13]. I.G. Fantus, S. Kadota, G. Deragon, B. Foster and B.I. Posner, *Biochemistry* 1989, **28**,
- 15 902 8864.
- 16
17 903
- 18
19 904 [14]. W. J. Geary. *Coord. Chem. Rev.* 1971, **7**, 81.
- 20
21 905
- 22
23 906 [15]. M. Samsonowicz, T. Hrynaszkiewicz, R. Świsłocka, E. Regulska and W.
- 24 907 Lewandowski, *J. Mol. Struct.* 2005, **744–747**, 345.
- 25
26 908
- 27
28 909 [16]. U. Blum and G. Schwedt. *Anal. Chim. Acta* 1998, **360**, 101.
- 29
30 910
- 31
32 911 [17]. E.G. Ferrer, A. Bosch, O. Yantorno and E.J. Baran. *Bioorg. Med. Chem.* 2008, **16**,
- 33 912 3878.
- 34
35 913
- 36
37 914 [18]. M. Shahlaei, B. Rahimi, A. Nowroozi and M.R. Ashrafi-Kooshk. *Chem-Biol Interact.*
- 38 915 2015, **242**, 235.
- 39
40 916
- 41
42 917 [19]. M.J. Frisch, G.W. Trucks, H.B. Schlegel, G.E. Scuseria, M.A. Robb, J.R.
- 43 918 Cheeseman, G. Scalmani, V. Barone, B. Mennucci, G.A. Petersson, H. Nakatsuji, M.
- 44 919 Caricato, X. Li, H.P. Hratchian, A.F. Izmaylov, J. Bloino, G. Zheng, J.L. Sonnenberg, M.
- 45 920 Hada, M. Ehara, K. Toyota, R. Fukuda, J. Hasegawa, M. Ishida, T. Nakajima, Y. Honda,
- 46 921 O. Kitao, H. Nakai, T. Vreven, J.A. Montgomery Jr., J.E. Peralta, F. Ogliaro, M. Bearpark,

- 1
2
3 922 J.J. Heyd, E. Brothers, K.N. Kudin, V.N. Staroverov, T. Keith, R. Kobayashi, J. Normand, New Article Online
DOI: 10.1039/C9NJ01638D
- 4
5 923 K. Raghavachari, A. Rendell, J.C. Burant, S.S. Iyengar, J. Tomasi, M. Cossi, N. Rega, J.M.
6
7 924 Millam, M. Klene, J.E. Knox, J.B. Cross, V. Bakken, C. Adamo, J. Jaramillo, R.
8
9 925 Gomperts, R.E. Stratmann, O. Yazyev, A.J. Austin, R. Cammi, C. Pomelli, J.W. Ochterski,
10
11 926 R.L. Martin, K. Morokuma, V.G. Zakrzewski, G.A. Voth, P. Salvador, J.J. Dannenberg, S.
12
13 927 Dapprich, A.D. Daniels, O. Farkas, J.B. Foresman, J.V. Ortiz, J. Cioslowski and D.J. Fox,
14
15 928 Gaussian 09, Revision B.01, Gaussian, Inc, Wallingford CT, 2010.
16
17 929
18
19 930 [20]. Y. Zhao and D.G. Truhlar, *Theor. Chem. Acc.* 2007, **120**, 215.
20
21 931
22
23 932 [21]. M.E. Casida, Recent developments and applications in modern density functional
24
25 933 theory, in: J.M. Seminario (Ed.), *Theor. Comput. Chem*, vol. 4, Elsevier, Amsterdam,
26
27 934 1996.
28
29 935
30
31 936 [22]. A.D. Becke, *Phys. Rev. A* 1988, **38**, 3098.
32
33 937
34
35 938 [23]. C. Lee, W. Yang and R.G. Parr, *Phys. Rev. B.* 1988, **37**, 785.
36
37 939
38
39 940 [24]. K. Nakamoto, *Infrared and Raman Spectra of Inorganic and Coordination*
40
41 941 *Compounds: Part A: Theory and Applications in Inorganic Chemistry*, Sixth Edition, 2009,
42
43 942 John Wiley and Sons.
44
45 943
46
47 944 [25]. J. Selbin. *Coord. Chem Rev.* 1996, **1**, 293.
48
49 945
50
51 946 [26]. S. Pacigová, R. Gyepes, J. Tatiersky and M. Sivák. *Dalton Trans.*, 2008, 121.
52
53 947
54
55
56
57
58
59
60

- 1
2
3 948 [27]. Infrared Spectral Interpretation. A systematic approach. B. Smith, 1999, CRC press, View Article Online
4 949 LLC. DOI: 10.1039/C9NJ01638D
5
6
7 950
8
9 951 [28]. R. Swisłocka, M. Samsonowicz, E. Regulska and W. Lewandowski, *J. Mol. Struct.*,
10 952 2006, **792-793**, 227.
11
12
13 953
14 954 [29]. (a) A. E. Gerbase, M. Martinelli, L. G. Fagundes, V. Stefani and S. J. Da Silva, *J.*
15 955 *Coord. Chem.*, 1999, **47**,451. (b) S. Pacigová, R. Gyepes, J. Tatiersky, M. Sivák. *Dalton*
16 956 *Trans.* 2008, 121.
17
18 957
19 958 [30]. E. Lodyga-Chruscinska, D. Sanna, E. Garribba and G. Micera. *Dalton Trans.*, 2008,
20 959 4903.
21
22 960
23 961 [31]. J. Selbin, L. Morpurgo, *J. Inorg. Nucl. Chem.*, 1965, **27**, 673.
24 962
25 963 [32]. N.D. Chasteen (1981) In: Berliner LJ, Reuben J (eds) Biological magnetic resonance,
26 964 vol 3. Plenum, New York.
27 965
28 966 [33]. G.R. Hanson, Y. Sun and C. Orvig. *Inorg. Chem.* 1996, **35**, 6507.
29 967
30 968 [34]. T. Jakusch, W. Jin, L. Yang, T. Kiss and D.C. Crans. *J. Inorg. Biochem.* 2003, **95**,1.
31 969
32 970 [35]. N. Mitic, S.J. Smith, A. Neves, L.W. Guddat, L.R. Gahan and G. Schenk. *Chem. Rev.*
33 971 2006, **106**, 3338.
34 972
35 973 [36]. C.C. McLauchlan, J.D. Hooker, M.A. Jones, Z. Dymon, E.A. Backhus, B.A. Greiner,
36 974 N.A. Dorner, M.A. Youkhana and L.M. Manus. *J. Inorg. Biochem.* 2010, **104**, 274.

- 1
2
3 975 [37]. M. Li, W. Ding, B. Baruah, D.C. Crans and R. Wang, *J. Inorg. Biochem.* 2008, **102**, 1846.
4 1846.
5
6 976
7 977
8
9 978 [38]. J.J. Boruah, D. Kalita, S.P. Das, S. Paul and N.S. Islam, *Inorg. Chem.* 2011, **50**, 8046.
10 979
11
12 980 [39]. H. Sugiyama, S. Matsugo, H. Misu, T. Takamura, S. Kaneko, Y. Kanatani, M. Kaido,
13 C. Mihara, N. Abeywardana, A. Sakai, K. Sato, Y. Miyashita and K. Kanamori, *J. Inorg.*
14 *Biochem.* 2013, **121**, 66.
15
16 981
17
18 982
19
20 983
21
22 984 [40]. A. Ziegler, J. Florián, M.A. Ballicora and A.W. Herlinger, *J. Enzyme Inhibit Med.*
23 *Chem.* 2009, **24**,
24
25 985
26
27 986
28
29 987 [41]. C.M. Vescina, V.C. Sálice, A.M. Cortizo and S.B. Etcheverry, *Biol Trace Element*
30 *Res.* 1996, **53**, 185.
31
32 988
33
34 989
35
36 990 [42]. P. J. Stankiewicz and M.J. Gresser, *Biochemistry* 1988, **27**, 206.
37
38 991
39
40 992 [43] D.C. Crans, J.J. Smee, E. Gaidamauskas and L. Yang, *Chem. Rev.* 2004, **104**, 849.
41
42 993
43
44 994 [44] D. Crans, *J. Org. Chem.* 2015, **80**, 11899.
45
46 995
47
48 996 [45] A.P. Seale, L.A. de Jesus, S-Y Kim, Y-H Choi, H.B. Lim, C.-S Hwang and Y-S. Kim,
49 *Biotechnol. Lett.* 2005, **27**, 221.
50
51 997
52
53 998
54
55 999 [46] L. Lu, X. Gao, M. Zhu, S. Wang, Q. Wu, S. Xing, X. Fu, Z. Liu and M. Guo,
56 *Biometals* 2012, **25**, 599.
57
58 1000
59
60

- 1
2
3 1001 [47] J.D. Siqueira, A.C.O. Menegatti, H.Terenzi, M.B. Pereira, D. Roman, E.F. Rosso, *View Article Online*
4 *DOI: 10.1039/C9NJ01638D*
5 1002 P.C. Piquini, B.A. Iglesias and D.F. Back, *Polyhedron*, 2017, **130**, 184.
6
7 1003
8
9 1004 [48] J.J. Boruah, D. Kalita, S.P. Das, S. Paul and N.S. Islam, *Inorg. Chem.* 2011, **50**, 8046.
10
11 1005
12
13 1006 [49] A. Morinville, D. Maysinger and A. Shaver, *TiPS* 1998, **19**, 452.
14
15 1007
16
17 1008 [50] D.C. Crans, A.D. Keramidas, C. Drouza, *Phosphorus Sulfur Silicon Relat. Elem.* 1996,
18
19 **109**, 245.
20
21 1009
22
23 1010
24
25 1011 [51]. B. Lendl, P. Krieg and R. Kellner, *Fresenius J. Anal. Chem.* 1998, **360**, 717.
26
27 1012
28
29 1013 [52]. R. Vonach, B. Lendl and R. Kellner, *Analyst.*, 1997, **122**, 525.
30
31 1014
32
33 1015 [53]. P.T.T. Wong and D.W. Armstrong, *Biochim. Biophys. Acta*, 1992, **1159**, 237.
34
35 1016
36
37 1017 [54]. L. de La Fourniere, O. Nosjean, R. Buchet and B. Roux, *Biochim. Biophys. Acta*,
38
39 1018 1995, **1248**, 186.
40
41 1019
42
43 1020 [55]. M. Bortolato, F. Besson and B. Roux, *PROTEINS: Structure, Function, and Genetics*
44
45 1021 1999, **37**, 310.
46
47 1022
48
49 1023 [56]. S. Bem and W.S. Ostrowski, *Acta Biochim. Pol.* 2001, **48**, 755.
50
51 1024
52
53 1025 [57]. R. Gilmanishin, S. Williams, R.H. Callender, W.H. Woodruff and R. B. Dyer, *Proc.*
54
55 1026 *Natl. Acad. Sci. USA*, 1997, **94**, 3709.
56
57 1027
58
59
60

1
2
3 1028 [58]. K. Murayama and M. Tomida, *Biochem.* 2004, **43**, 11526.

View Article Online
DOI: 10.1039/C9NJ01638D

4
5 1029

6
7 1030 [59]. J.R. Lakowicz. Principles of fluorescence spectroscopy. New York: Plenum Press;

8
9 1031 1983. p. 266e7.

10
11 1032

12
13 1033 [60]. U. Kragh-Hansen, V.T.G. Chuang and M. Otagiri, *Biol. Pharm. Bull.*2002, **25** 695.

14
15 1034

16
17 1035 [61]. P.D. Ross, S. Subramanian, *Biochem.* 1981, **20**, 3096.

18
19 1036

20
21 1037 [62]. Y. Wang, X. Wang, J. Wang, Y. Zhao, W. He and Z. Guo, *Inorg. Chem.* 2011, **50**,

22
23 1038 12661.

24
25 1039

26
27 1040 [63]. Z. Mandegani, Z. Asadi, M. Asadi, H.R. Karbalaeei-Heidari and B. Rastegari, *Dalton*

28
29 1041 *Trans.*, 2016, **45**, 6592.

30
31 1042

32
33 1043 [64]. Y. Wang, X. Wang, J. Wang, Y. Zhao, W. He and Z. Guo. *Inorg. Chem.* 2011, **50**,

34
35 1044 12661.

36
37 1045

38
39 1046

40
41 1047

42
43

44
45

46
47

48
49

50
51

52
53

54
55

56
57

58
59

60

1048 **Table 1.** Selected bond lengths (Å) and angles (°) around vanadium in the aminobenzoate
 1049 (L) oxidovanadium complexes complex calculated at B3LYP 6-311+g*level of theory.

<i>cis</i> -[VOL ₂ H ₂ O] ^a				[VO(O ₂)L(H ₂ O)].H ₂ O			
Bond lengths (Å)		angles (°)		Bond lengths (Å)		angles (°)	
V-O1	1.597	O1VO2	110.2	V-O1	1.589	O1VO2	107.4
V-O2	2.016	O1VO3	108.5	V-O2	1.998	O1VO3	98.3
V-O3	2.017	O1VO4	103.2	V-O3	2.060	O1VO4	109.9
V-O4	2.021	O1VO5	158.9	V-O4	1.826	O1VO5	109.1
V-O5	2.269	O1VO _w	93.8	V-O5	1.834	O1VO _w	97.2
V-O _w	2.129	O2VO3	65.3	V-O _w	2.122	O2VO3	64.3
		O2VO4	144.9			O2VO4	133.4
		O2VO5	88.7			O2VO5	138.5
		O2VO _w	93.4			O2VO _w	76.4
		O3VO4	94.3			O3VO4	83.4
		O3VO5	87.5			O3VO5	127.4
		O3VO _w	153.1			O3VO _w	140.5
		O4VO5	60.9			O4VO5	45.6
		O4VO _w	95.0			O4VO _w	124.3
		O5VO _w	75.2			O5VO _w	80.2

1050 ^aFor the denomination of the atoms see Figure 1.

1051

1052

1053 **Table 2.** Characteristic FTIR bands for 4-aminobenzoic acid), its sodium salt,
 1054 $[\text{VO}(\text{O}_2)\text{L}(\text{H}_2\text{O})]\cdot\text{H}_2\text{O}$ and the calculated *cis*- and *trans*- $[\text{VOL}_2\text{H}_2\text{O}]$ isomers.(L=4-
 1055 aminobenzoate ligand).

New Article Online
 DOI: 10.1039/C9NJ01638D

Aminobenzoic acid	Benzoate sodium salt	[VOL ₂ H ₂ O]			[VO(O ₂)L(H ₂ O)].H ₂ O		Assignments Main contributions
		Exp	Calc. cis	Calc. trans	Exp	Calc.	
1680(s)							$\nu(\text{C}=\text{O}), (\text{COOH})$
1626(s)	1633(s)	1693(w) 1634(sh)	1667.47 1659.57 1667.75 1659.67	1666.67 1657.46	1696(s)	1663.28 1655.26	$\nu(\text{CC}), \delta(\text{NH}_2)$
				1653.35	1603(m)	1637.82	$\delta\text{H}_2\text{O}$
1600(s)	1591(s)	1604(br.s)	1626.06 1615.11		1590(m)	1600.66	$\nu(\text{CC}), \delta\text{H}_2\text{O}$
				1572.29			$\nu(\text{CC}), \delta(\text{HCC})$
1522(s)	1529(vs)	1530(sh) 1506(m)	1525.37 1462.97		1525(m) 1498(w)	1574.35 1508.78	$\nu_{\text{as}}(\text{COO}^-), \nu(\text{CC}), \delta(\text{HCC})$
				1466.22 1454.07	1460(sh)	1479.87	$\nu_{\text{as}}(\text{COO}^-), \nu(\text{CC}), \delta(\text{HCC})$
	1397(s)	1408(s) 1390(sh)	1431.35 1396.85		1429(s)	1434.09	$\nu_{\text{s}}(\text{COO}^-), \nu(\text{CC}),$
1317(m)	1285(sh)	1315(w)	1359.07 1348.50	1359.77 1334.06	1378(m) 1315(sh) 1265(s)	1363.98 1326.21	$\nu(\text{NC}), \delta(\text{HCC})$
1171(s)	1173(s)	1181(m)	1208.34 1205.26	1206.39 1173.85	1185(sh) 1176(m)	1206.99 1170.38	$\nu(\text{CC}), \delta(\text{HCC})$
1127(m)	1136(m)	1120(m) 1016(m)	1166.09	1155.48 1069.87	1127(m) 1112(m)	1151.31	$\nu(\text{CC}), \delta(\text{HCC})$
1072(w)	1083(m)	1101(m)	1151.67 1073.24		1069(w)	1055.09	$\delta(\text{HCC}), \delta(\text{HNC})$
		965(s)	1007.74	1014.48			$\nu(\text{V}=\text{O})$
					1017(m)	1021.06	$\delta(\text{CCC})$

1

2

3						998(m)	979.96	View Article Online DOI: 10.3390/nj10110047
4								$\nu(\text{V=O})+\nu(\text{O=O})$
5						901(w)	884.92	$\delta(\text{CCC}), \delta(\text{OCO}) \nu(\text{CC}),$
6						871(m)	865.84	$\tau(\text{HCCC}), \tau(\text{CCCC}),$ $\gamma(\text{OCOC})$
7								$\tau(\text{HCCC}), \gamma(\text{OCOC})$
8		853(m)	868.90					
9								$\tau(\text{HCCC}), \gamma(\text{OCOC})$
10								$\delta(\text{CCC}), \gamma(\text{NCCC})$
11					868.68			$\delta(\text{CCC})$
12								$\delta(\text{CCC}), \delta(\text{OCO})$
13						844(m)	838.75	$\delta(\text{CCC}), \delta(\text{OCO})$
14								$\nu(\text{CC}), \delta(\text{OCO}), \delta(\text{CCC})$
15		829(m)	838.93					$\delta(\text{OCO}), \delta(\text{CCC})$
16					835.56			
17								$\delta(\text{CCV}),$
18		769(m)	803.42					$\tau(\text{HCCC}), \gamma(\text{OCOC})$
19					803.19			
20								$\delta(\text{OCO})$
21		668(w)	664.87	653.90				$\delta(\text{HOV})$
22		638(w)	626.00					
23						691(m)	680.96	$\tau_{\text{H}_2\text{O}}, \delta(\text{CCC}), \nu(\text{VO}_2)$
24						668(m)	663.34	
25						658(w)	660.60	
26						630(m)	625.18	$\delta(\text{OOV}), \nu(\text{VO}_2)$
27		542(w)	519.67					$\tau_{\text{H}_2\text{O}}, \tau(\text{HCC})$
28					518.50			$\gamma(\text{NCCC})$
29						560(m)	566.08	$\delta(\text{CCO}), \delta(\text{COV}), \tau(\text{H}_2\text{O})$
30						538(m)		
31								$\tau(\text{HOVC})$
32		507(w)	502.18					
33								$\nu(\text{V-C}), \tau(\text{HOVC})$
34					509.36		478.62	

46

47 1056 vs= very strong, s = strong, m = media, w = weak, vw = very weak, sh=shoulder, ν =48 1057 stretching, δ = in-plane bending, γ = out-of-plane bending, τ =torsion.

49

50 1058

51

52

53

54

55

56

57

58

59

60

61

62

63

64

65

66

67

68

69

70

71

72

1059 **Table 3.** IC₅₀ and K_m data values for a series of vanadium(IV) and (V) complexes
 1060 containing NH group and/or comprising phenyl group structurally related to PNPP
 1061 substrate.

View Article Online
 DOI: 10.1039/C9NJ01638D

Phosphatase	Compound	IC ₅₀ (μM)	K _m (μM)	
AcP ^a (sodium acetate, pH=4.8)	VO(imc) ₂	-	3.3	[36]
	VO ₂ (imc) ₂ ⁻	-	33	[36]
	VO(anc) ₂	-	23	[36]
	VO ₂ (anc) ₂ ⁻	-	0.25	[36]
AcP ^b (acetate, pH=5.6)	V(IV)O ²⁺	67.37	-	This work
	[VO(O ₂) ⁺	63.45	-	This work
	[VOL ₂ H ₂ O]	250	-	This work
	[VO(O ₂)L(H ₂ O)]	No inhibition	-	This work
ALP ^c (Tris, pH=7.8)	VO(imc) ₂	-	15.0	[36]
	VO ₂ (imc) ₂ ⁻	-	12.6	[36]
	VO(anc) ₂	-	68	[36]
	[VO(Big) ₂].H ₂ O	33	-	[44]
	[VO(Big1) ₂].2H ₂ O	17	-	[44]
	V(IV)O ²⁺	>500 μM	-	This work
	[VO(O ₂) ⁺	No inhibition	-	This work
	[VOL ₂ H ₂ O]	No inhibition	-	This work
	[VO(O ₂)L(H ₂ O)]	500 μM	-	This work
ALP ^d (Glycine, pH=10)	Na[VO(O ₂) ₂ (H ₂ O)]	25.18	9.13	[47]
	[VO(O ₂) ₂ (sulfonate)]-PSS	45.25	54.50	[47]
	V ₂ O ₂ (O ₂) ₄ -(carboxylate)- VO(O ₂) ₂ (sulfonate)]-PSSM	52.54	59.98	[47]
ALP ^e (HEPES, pH=8)	NH ₄ [VO(O ₂)(dipic)(H ₂ O)]	-	13.0	[49]
PTP1B (HEPES, pH=7.3)	VO(imc) ₂	-	43	[36]
	VO ₂ (imc) ₂ ⁻	-	12.5	[36]
	VO(anc) ₂	-	56.7	[36]
	VO ₂ (anc) ₂ ⁻	-	19.3	[36]
PTP1B (MOPS, pH=7)	[VO(Big) ₂].H ₂ O	8.6 x 10 ⁻⁴	-	[45]
	[VO(Big1) ₂].2H ₂ O	10.5 x 10 ⁻⁴	-	[45]
	VO(trp) ₂	0.76	-	[43]
	VO(hino) ₂	0.27	0.15	[43]
PTP1B (imidazole, pH = 7.0)	[VO ₂ (L ¹) ₂](Et) ₃ NH ₂	1.51	-	[46]
	[VO ₂ (L ²) ₂](DBU-H) ₂	lower inhibition	-	[46]

1062 ^aWheat Germen, ^bPotato source, ^cBovine calf intestine, MOPS pH = 7 for biguanido complexes
 1063 and, ^dALP = rabbit intestine, ^eALP = chicken intestine, PTP1B = Protein-tyrosine phosphatase 1B.
 1064 L = 4-aminobenzoate, imc = imidazole-4-carboxylate, anc = anthranilate (2-aminobenzoate); trp =
 1065 tropolonato; hino = hinokitolonato, dipic = dipicolinic acid. HBig.HCl = N',N'-dimethylbiguanide
 1066 hydrochloride, Big1 = phenformin, see scheme. PSS = poly(sodium 4-styrene sulfonate), PSSM =
 1067 poly(sodium styrene sulfonate-*co*-maleate)]. L¹ = 2,4-(dihydroxyphenyl)ethylidene)benzohydrazide,
 1068 L² = bis[(3-hydroxy-5-(hydroxymethyl)-2-methylpyridin-4-yl)methylene]oxalohydrazide; (Et)₃NH =
 1069 triethylamine; DBU = 1,8-diazabicyclo[5.4.0]undec-7-ene.
 1070

1071 **Table 4.** FT-IR/ATR determination of secondary structure percentages of (i) ALP (glycine
 1072 buffer pH=10.5) and (ii) AcP (acetate buffer) of the systems containing ALP with 4-
 1073 aminobenzoic acid (ALP-L), V(IV)O²⁺ (ALP-VO), oxidovanadium (ALP-[VOL₂H₂O]) and
 1074 peroxidovanadium (ALP-[VO(O₂)L(H₂O)].H₂O) compound (500 μM).
 1075

Alkaline Phosphatase				
Amide I components	% ALP-control	% ALP-L	% ALP-[VOL ₂ H ₂ O]	% ALP-[VO(O ₂)L(H ₂ O)].H ₂ O
β-antiparallel 1675-1695	3.41±0.03	9.74±0.07	8.21±0.06	8.94±0.07
Turns 1666-1673	10.99±0.13	6.20±0.05	8.82±0.07	7.57±0.03
α-helix 1650-1658	39.59±0.45	34.25±0.41	33.08±0.38	24.22±0.30
Random coil 1637-1645				
Solvated helix 1625-1637	24.9±0.29	29.87±0.31	30.17±0.36	36.77±0.22
β-sheet 1613-1625	21.10±0.17	19.97±0.18	24.09±0.20	22.37±0.27
Acid Phosphatase				
Amide I components	% AcP-control	% AcP-L	% AcP-[VOL ₂ H ₂ O]	% AcP-[VO(O ₂)L(H ₂ O)].H ₂ O
β-antiparallel 1675-1695	7.60±0.20	13.05±0.27	14.87±0.23	12.94±0.25
Turns 1666-1673	16.95±0.31	9.98±0.17	15.10±0.32	12.02±0.19
α-helix 1650-1658	34.37±0.80	29.96±0.90	20.77±0.57	32.06±0.64
Random coil 1637-1645	26.8±0.38	25.01±0.56	21.41±0.35	26.57±0.42
Solvated helix 1625-1637	5.31±0.03	5.35±0.08	21.85±0.27	3.26±0.10
β-sheet 1613-1625	8.98±0.18	16.65±0.33	5.97±0.16	12.97±0.26

1076 Averages (triplicates from separate samples) ±SE.

1077

1078 **Table 5:** 3D Fluorescence Spectral Parameters of BSA, 4-amino benzoic acid-BSA and
 1079 oxidovanadium(IV) complex-BSA system.

1080

1081 **BSA**

Peak position	$\lambda_{ex}/\lambda_{em}$ (nm/nm)	$\Delta\lambda$	Intensity
Peak A	280/337.9	57.9	4956.4
Peak B	230/340.7	110.7	575.8

1082

1083 **4-amino benzoic acid-BSA system**

Peak position	$\lambda_{ex}/\lambda_{em}$ (nm/nm)	$\Delta\lambda$	Intensity
Peak A	280/335.5	55.5	5721.2
Peak B	230/337.5	107.5	644.6

1084

1085

1086 **Oxidovanadium(IV)complex-BSA system**

Peak position	$\lambda_{ex}/\lambda_{em}$ (nm/nm)	$\Delta\lambda$	Intensity
Peak A	280/337.2	57.2	5340.3
Peak B	230/-	-	-

1087

1088

1089

1090

1091

1092

1093

Figure 1

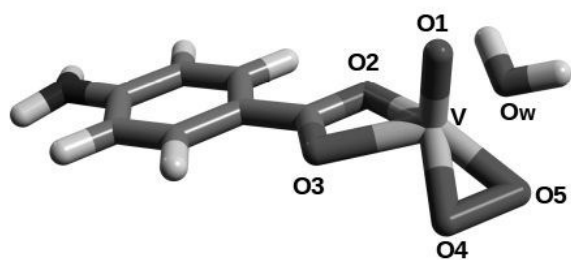
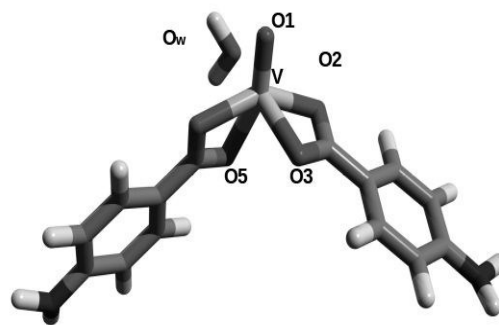
View Article Online
DOI: 10.1039/C9NJ01638D(A) [VO(O₂)(C₇H₆NO₂)(H₂O)].H₂O([VO(O₂)L(H₂O)].H₂O)(B) *cis*-VO(C₇H₆NO₂)₂.H₂O(VOL₂H₂O)

Figure 2.

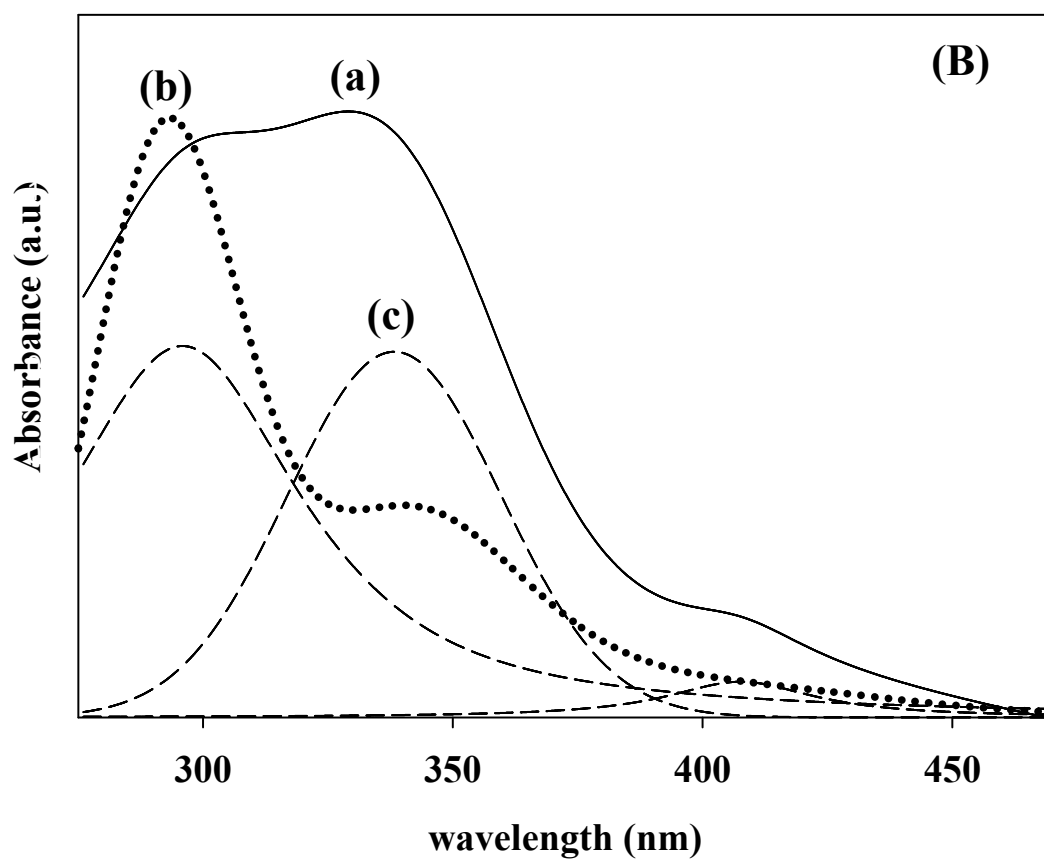
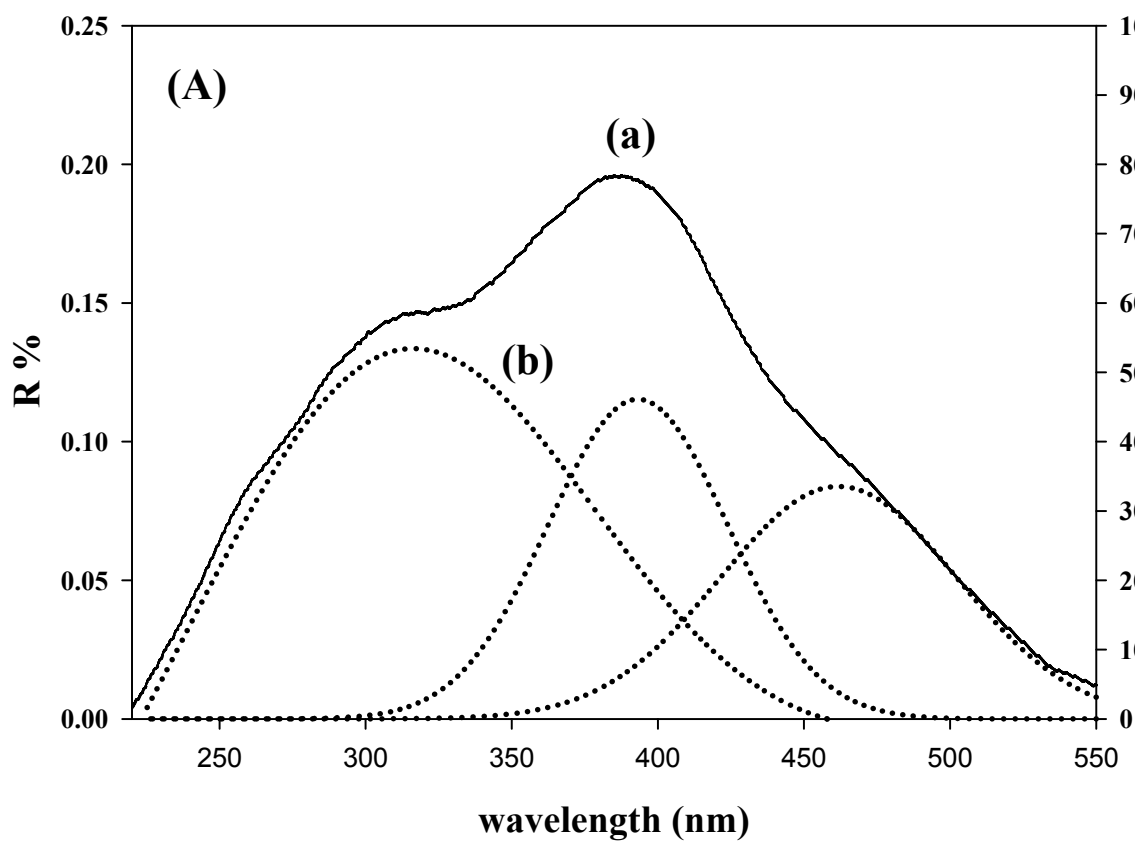
View Article Online
DOI: 10.1039/C9NJ01638D

Figure 3.

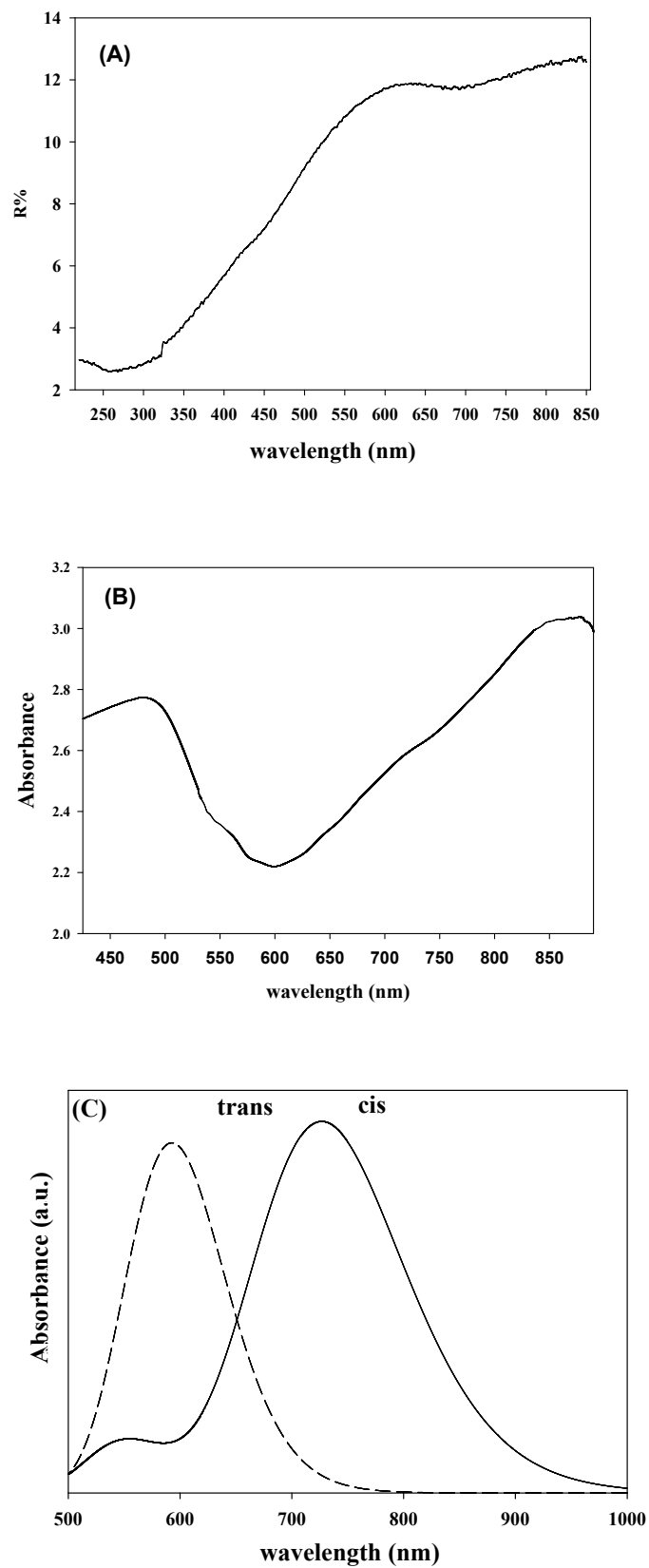
View Article Online
DOI: 10.1039/C9NJ01638D1
2
3
4
5
6
7
8
9
10
11
12
13
14
15
16
17
18
19
20
21
22
23
24
25
26
27
28
29
30
31
32
33
34
35
36
37
38
39
40
41
42
43
44
45
46
47
48
49
50
51
52
53
54
55
56
57
58
59
60

Figure 4

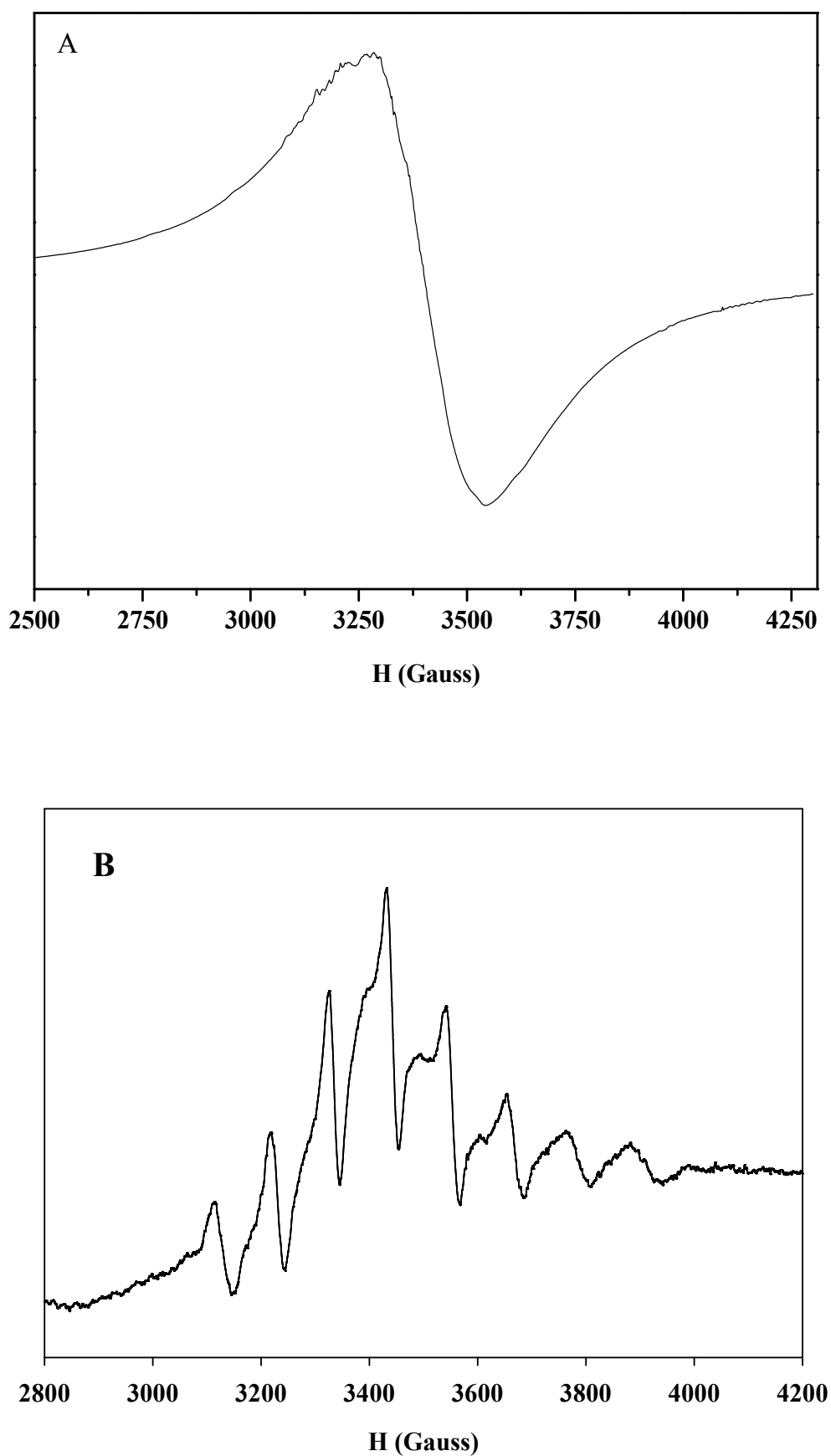
View Article Online
DOI: 10.1039/C9NJ01638D

Figure 5

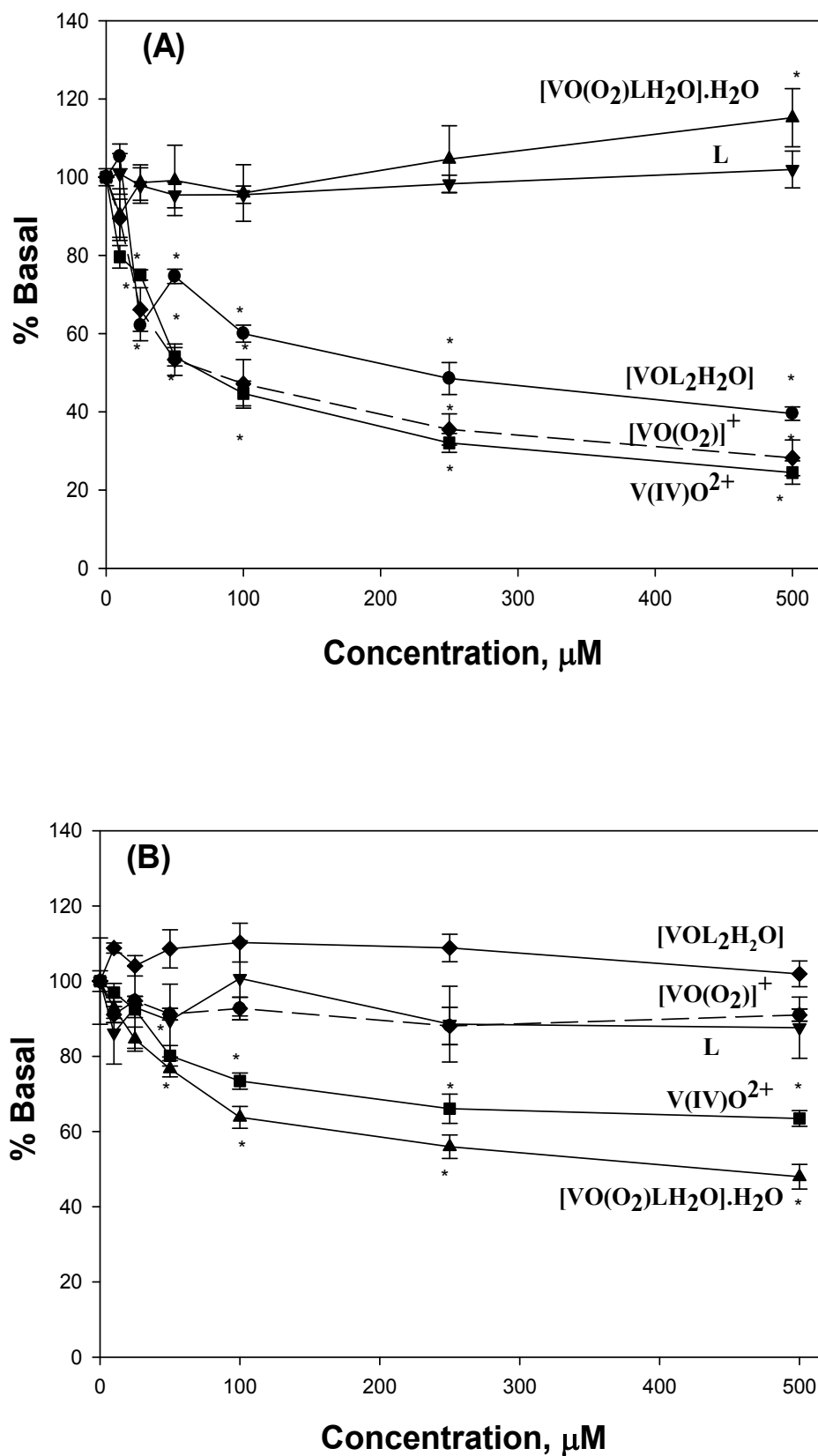


Figure 6.

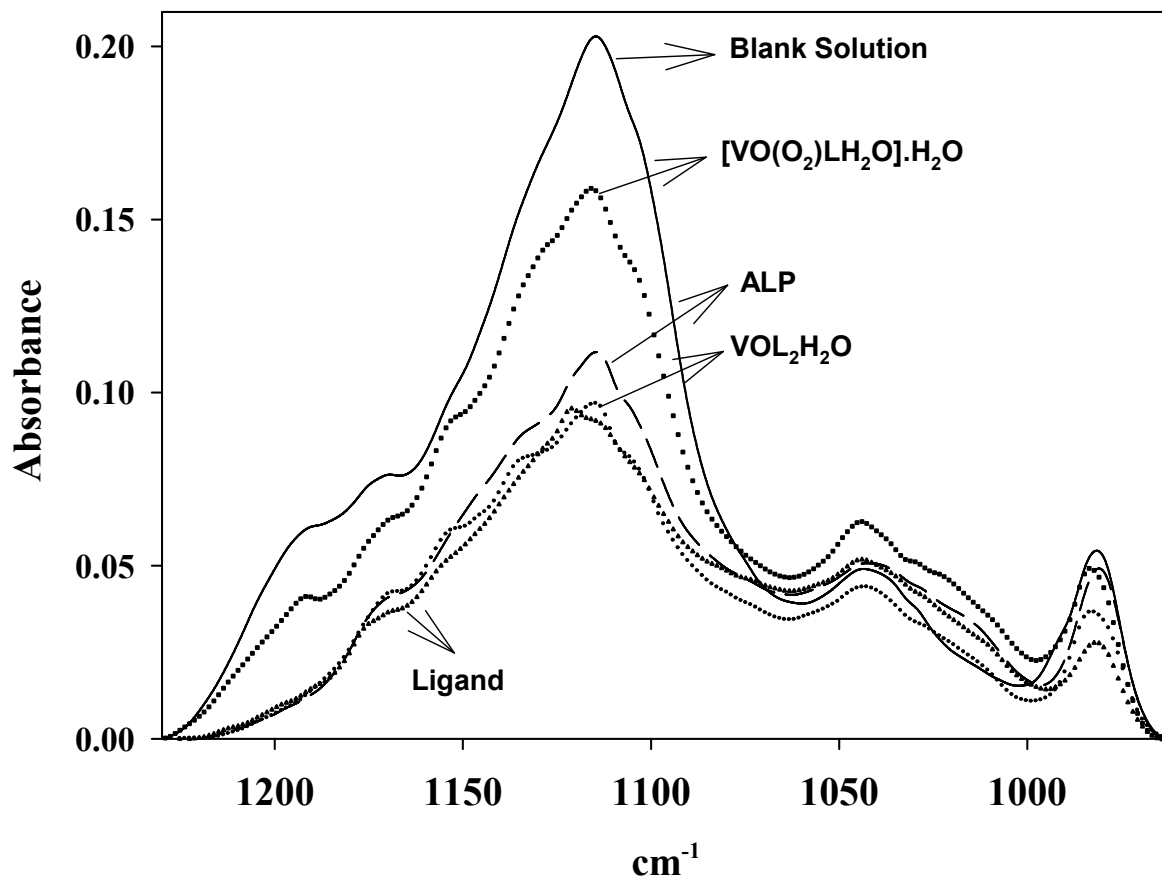
View Article Online
DOI: 10.1039/C9NJ01638D

Figure 7

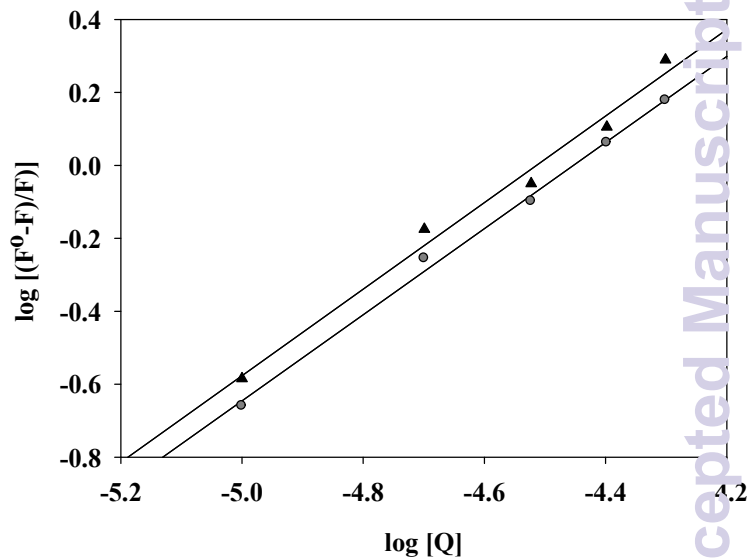
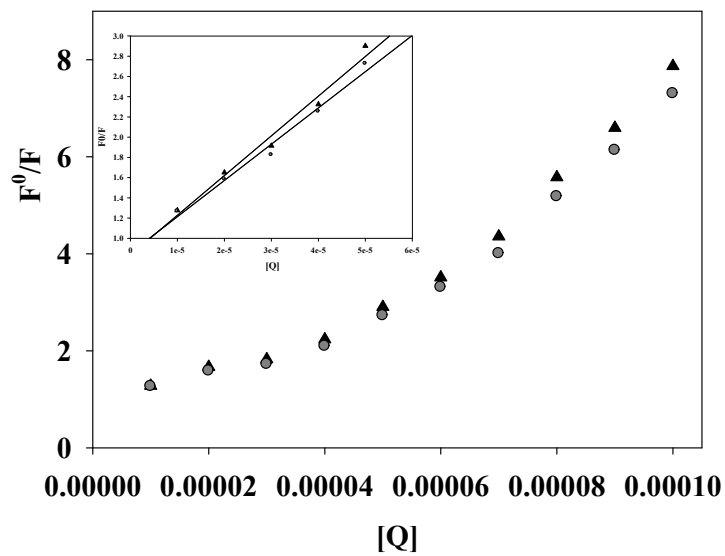
View Article Online
DOI: 10.1039/C9NJ01638D

Figure 8

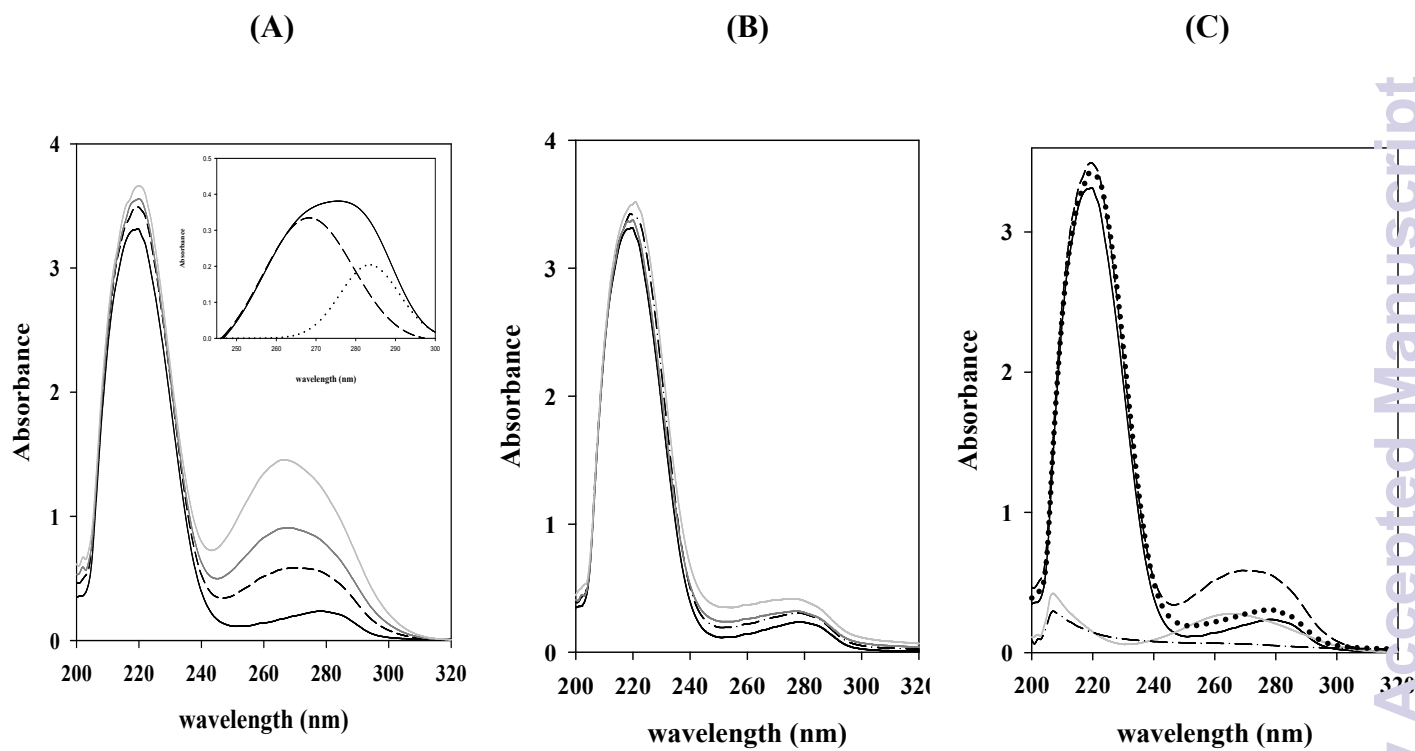
View Article Online
DOI: 10.1039/C9NJ01638D

Figure 9

